HHS Public Access

ATF7ip targets transposable elements for H3K9me3 deposition to modify CD8+ T cell effector and memory responses

Jun Hyung Sin[*,†,‡,1], **Sujit Kashyap**[*,†,1], **Dante Acenas**[§], **Jessica T. Cortez**[§,¶], **James Lee**[‖,#], **Alexander Marson**[‡,§,**,††,‡‡,§§], **Mehrdad Matloubian**[#,¶¶], **Michael R. Waterfield**[*,†,‡]

[*]Division of Pediatric Rheumatology, University of California San Francisco, San Francisco, California 94143-0795, USA.

[†]Department of Pediatrics, University of California San Francisco, San Francisco, California 94143-0795, USA.

[‡]Biomedical Sciences Graduate Program, University of California, San Francisco, CA 94143, USA

[§]Diabetes Center, University of California, San Francisco, San Francisco, California 94143-0795, USA

[¶]Present Address: Sonoma Biotherapeutics, 400 E. Jamie Ct, Suite 250, South San Francisco CA 94080

[‖]Division of Hematology and Oncology, University of California, San Francisco, San Francisco, CA 94143, USA.

[#]Department of Medicine, University of California San Francisco, San Francisco, California 94143-0795, USA.

[**]J. David Gladstone Institutes, San Francisco, CA 94158, USA

[††]Parker Institute for Cancer Immunotherapy, San Francisco, CA 94129, USA

[‡‡]UCSF Helen Diller Family Comprehensive Cancer Center, University of California, San Francisco, CA 94158, USA

[§§]Chan Zuckerberg Biohub, San Francisco, CA 94158, USA

[¶¶]Division of Rheumatology, University of California San Francisco, San Francisco, California 94143-0795, USA.

Abstract

CD8+ T cells are critical for the immune response to pathogens and tumors and CD8+ T cell memory protects against repeat infections. Here, we identify the activating transcription factor 7 interacting protein (ATF7ip) as a critical regulator of CD8+ T cell immune responses. Mice

with a T cell specific deletion of ATF7ip have a CD8+ T cell intrinsic enhancement of *Il7r* expression and *Il2* expression leading to enhanced effector and memory responses. ChIP-seq studies identified ATF7ip as a repressor of *Il7r* and *Il2* gene expression through the deposition of the repressive histone mark H3K9me3 at the *Il7r* gene and *Il2-Il21* intergenic region. Interestingly, ATF7ip targeted transposable elements (TE) for H3K9me3 deposition at both the *IL7r* locus and *Il2-Il21* intergenic region indicating that ATF7ip silencing of TE is important for regulating CD8+ T cell function. These results demonstrate a new epigenetic pathway by which IL7r and IL-2 production are constrained in CD8+ T cells, and this may open up new avenues for modulating their production.

Introduction:

CD4+ and CD8+ T cells are important mediators of adaptive immunity. CD4+ T cells provide help in the form of cytokines while CD8+ T cells eliminate viral infected cells and tumor cells. Due to the function of CD8+ T cells in the clearance of infectious organisms and tumors, there has been a large body of work over the last two decades characterizing the factors important for CD8+ effector T cell function and the generation of memory T cells(1–3). Critical effector molecules of CD8+ T cells include granzymes and the effector cytokines IL-2, TNFα, and IFNγ. After a primary infection, a subset of CD8+ T cells become memory CD8+ T cells that require stromal cell derived interleukin-7 (IL-7) signaling for their induction and maintenance(4). Secondary to their requirement for IL-7, memory CD8+ T cells are marked by the expression of the IL7r and memory precursor cells can be identified early after infection based on increased IL7r expression(5). Conversely, CD8+ terminal effector cells are marked by high levels of Killer Cell Lectin Like Receptor G1 (KLRG1) and mediate pathogen clearance(6). Recent studies have delineated the transcription factors critical for terminal effector and memory precursor formation with T box transcription factor 1 (TBET) essential for terminal effector formation and Eomesodermin (Eomes) and T cell factor 1 (TCF1) important in memory precursor formation(6–8). While the transcription factor networks for CD8+ effector and memory formation are established, less is known about the epigenetic regulation of CD8+ T cell differentiation.

Prior studies have characterized the effect of specific repressive histone modifications on effector T cell development (9). While generation of the repressive H3K27me3 histone mark in T cells relies on one protein complex centered on the histone methyltransferase, EZH2, there are multiple protein complexes required for the generation of the repressive H3K9me3 histone mark (10–12). Recent studies in CD8+ T cells has shown the importance of EZH2 in CD8+ T effector differentiation(13). Moreover, the H3K9me3 methyltransferase SUV39H1 has been shown to be essential for CD8+ T cell function by silencing a stem-cell gene program to allow a robust memory response(14). To address whether additional proteins important in the formation of the H3K9me3 histone mark modulate CD8+ T cell effector differentiation, we started to examine chromatin regulation in CD8+ T cell differentiation.

One protein known to be critical for chromatin regulation in T cells is the activating transcription factor 7 interacting protein (ATF7ip). ATF7ip is an epigenetic regulator involved in gene repression through promoting the formation of the H3K9me3 mark

(15). Multiple ATF7ip binding partners have been characterized including the histone methyltransferase SETDB1/ESET (15, 16), and members of the HUSH (human silencing hub) complex (17–20) and ATF7ip has been found to regulate gene expression programs in retroviral silencing, cellular senescence, cancer susceptibility, and immune tolerance (16, 21–23). Recent studies have also highlighted a specific function for ATF7ip in silencing transposable elements (TE) (16, 24, 25). TE are mobile, self-replicating, highly repetitive DNA elements that comprise approximately 50% of mammalian genomes(26). TE come in two classes with Class I TE consisting of the retrotransposons (endogenous retroviruses (ERVs), long interspersed nuclear elements (LINEs), and short interspersed nuclear elements (SINEs)) and Class 2 TE comprising DNA transposons(27). Initially thought to be primarily junk DNA that have seeded the genome over evolutionarily time, recent studies have found that TE have been co-opted in eukaryotic genomes to serve as important regulators of gene expression(28, 29). Because of the gene regulatory sequences contained within TEs there are mechanisms in place to silence ERVs (and other TE) through DNA methylation or H3K9me3 deposition over the TE sequence. Due to ATF7ip's well-characterized function in silencing TE through H3K9me3 deposition, we hypothesized that this pathway may be important in CD8+ T cells.

In order to characterize the in vivo function of ATF7ip in CD8+ T cell effector responses and in silencing TE, we utilized an *Atf7ip* conditional mouse line with a variety of models of infection. Surprisingly, we found that T cell specific deletion of ATF7ip in mice resulted in enhanced clearance of the pathogen Listeria Monocytogenes (LM). Furthermore, CD8+ T cell transfer studies and global gene expression studies revealed that there is a CD8+ T cell intrinsic increase in T cell memory with increased *Il7r* expression. Consistent with enhanced memory cell formation, T cell specific deletion of *Atf7ip* resulted in an enhanced memory response to LM. Prior studies in CD4+ T cells, showed that ATF7ip is critical for silencing *Il2* gene expression through H3K9me3 deposition in the *Il2-Il21* intergenic region(30). Interestingly, we also found that *Atf7ip* was critical for silencing *Il2* expression in CD8+ T cells and that deletion of *Atf7ip* in CD8+ T cells resulted in increased autocrine IL-2 production which could have implications for both CD8+ effector and memory responses. ChIP-seq for H3K9me3 in naïve CD8+ T cells further refined the mechanism of increased *Il7r* and *Il2* expression by showing decreased deposition of H3K9me3 at the *Il7r* and *Il2* locus. Interestingly, genomic regions of ATF7ip dependent H3K9me3 deposition were enriched in transposable elements (TE) indicating that failure to silence TE with *Atf7ip*-deletion results in altered gene expression. Thus, we have identified a novel pathway through which CD8+ effector and memory responses are modulated with ATF7ip silencing of TE required to fine-tune *Il7r* and *Il2* gene expression.

Materials and Methods

Mice-

Atf7ip^fl/fl^ mice were generated as previously described(30). *CD4*-Cre mice were provided by Jeff Bluestone (University of California, San Francisco, San Francisco, CA). P14 mice (with transgenic expression of H-2D^b–restricted TCR specific for LCMV glycoprotein GP$_{33-41}$) were provided Mehrdad Matloubian (University of California, San Francisco, San

Francisco, CA). Mice were maintained in the UCSF specific pathogen–free animal facility in accordance with the guidelines established by the Institutional Animal Care and Use Committee and Laboratory Animal Resource Center, and all experimental procedures were approved by the Laboratory Animal Resource Center at UCSF.

T cell differentiation -

T cells were enriched from spleen and lymph nodes using the MagniSort CD8 negative selection kit (Thermo). Naïve CD8+ T cells were isolated by flow cytometry based on the markers CD4+CD62L+CD44- and cultured for either 24hrs or 48hrs in a 96well flat bottom plate coated with 2 ug/ml anti-CD3(clone 2C11/Tonbo) and 2ug/ml anti-CD28(clone 37.51/Tonbo). After culture, cells were isolated for either RNA-seq, qPCR, Flow Cytometry, or ELISA.

Infections and antibody treatments.—*CD4*-Cre/*Atf7ip*$^{+/fl}$ mice and *CD4*-Cre/*Atf7ip*$^{fl/fl}$ mice were infected i.v. with a lethal dose of 2×10^4 colony forming units (CFU) of Listeria monocytogenes (LM) or infected i.p. with 2×10^5 plaque forming units (PFU) LCMV Armstrong strain. To assess for the effect of blocking IL-2, *CD4*-Cre/*Atf7ip*$^{+/fl}$ mice and *CD4*-Cre/*Atf7ip*$^{fl/fl}$ mice were injected i.p. on days −1, 1, and 3 with 150ug of IL-2 blocking antibody (clone S4B6, BioXcell) or isotype control (*InVivo*MAb rat IgG2a isotype control,BioXCell) and infected with 2×10^4 CFU LM on day 0. To analyze the memory response, *CD4*-Cre/*Atf7ip*$^{+/fl}$ mice and *CD4*-Cre/*Atf7ip*$^{fl/fl}$ (*Atf7ip*$^{fl/fl}$) mice were first infected with 2×10^5 PFU LCMV Armstrong strain and then after > 60 days mice were reinfected i.v. with 1×10^6 CFU of LM expressing the LCMV glycoprotein GP33–41 (LM33). To prepare LM33 for infection, LM33 stocks frozen at −80 C were grown overnight at 37 °C in Brain, Heart, Infusion (BHI) broth (Sigma) supplemented with 5 ug/ml Erythromycin. Overnight cultures were sub-cultured by diluting into fresh BHI broth supplemented with 5 ug/ml Erythromycin and grown for approximately 4 hours. Bacteria CFU was then quantified by measuring optical density at 600 nm. To determine bacterial burden in infected mice, organs (spleen/liver) were homogenized in sterile 0.1% Triton X-100 (SIGMA) in dH2O buffer and serial dilutions were plated on BHI agar containing 5 ug/ml erythromycin and colony forming units (CFU) / organ was calculated. LCMV Armstrong and Listeria Monocytogenes (LM) were kindly supplied by Mehrdad Matloubian (University of California, San Francisco, San Francisco, CA) and LM33 was supplied Shomyseh Sanjabi (University of California, San Francisco, San Francisco, CA).

T cell transfers -

2×10^4 P14+/CD45.1.2/ *Atf7ip*$^{fl/fl}$ CD8+ T cells or P14+/CD45.1/ *Atf7ip*$^{+/fl}$ CD8+ T cells were individually or co-transferred into CD45.2 C57Bl/6 hosts 1 day prior to LCMV infection. Flow cytometry based on CD45 was utilized to distinguish P14+ cells of specific genotypes. P14+ cells were analyzed at specific timepoints to characterize memory cell formation. To analyze the memory response using transferred P14+ cells two separate experiments were performed. First, mice that received single transfers of congenically distinct P14+ T cells (2×10^4 P14+/CD45.1.2/ *Atf7ip*$^{fl/fl}$ CD8+ T cells or P14+/CD45.1/ *Atf7ip*$^{+/fl}$ CD8+ T cells) were infected with 2×10^5 PFU LCMV Armstrong strain and then after 60 days reinfected with 1×10^6 CFU of LM33 to analyze the memory response. Second,

mice that received a co-transfer of P14+ cells (2×10^4 P14+/CD45.1.2+/ *Atf7ip*$^{fl/fl}$ CD8+ T cells and P14+/CD45.1+/ *Atf7ip*$^{+/fl}$ CD8+ T cells) were infected with LCMV Armstrong and then after 60 days P14+ cells were sorted based on expression of CD45.1 or CD45.1.2 and then 3×10^4 cells of each genotype were transferred IV into naïve B6 mice one day prior to infection with 8×10^4 CFU LM33. All transfer experiments were sex matched between donors and recipients.

Human CD4 T cell isolation/culture -

Primary human CD4+ T cells for all experiments were sourced from healthy donors from leukoreduction chamber residuals after Trima Apheresis (Vitalant) or from freshly drawn whole blood under a protocol approved by the UCSF Institutional Review Board (IRB no. 13–11950). Peripheral blood mononuclear cells were isolated from samples by Lymphoprep centrifugation (StemCell) using SepMate tubes (StemCell). CD4+ T cells were isolated from peripheral blood mononuclear cells by magnetic negative selection using the EasySep Human CD4+ T Cell Isolation Kit (StemCell). After isolation, CD4+ T cells were stimulated with ImmunoCult Human CD3/CD28/CD2 T Cell Activator (StemCell) per the manufacturer's protocol and electroporated after 48 hrs of stimulation. After electroporation, cells were cultured for 2 days in RPMI medium supplemented with 10% FBS, 50 μM 2-mercaptoethanol, 10 μM N-acetyl l-cysteine and 1% penicillin/streptomycin and allowed to expand for 7 days prior to replating and restimulation with Immunocult for 24 hours. After restimulation, supernatant was collected for ELISA and cells were collected for RNA isolation and genomic DNA isolation.

CRISPR -

RNPs for CRISPR were produced by complexing a two-component gRNA to Cas9 as previously performed (31). In brief, CRISPR RNAs (crRNAs) and trans-activating crRNAs (tracrRNAs), were purchased from IDT. Lyophilized RNA was resuspended in Nuclease-free Duplex Buffer (Integrated DNA Technologies) at a concentration of 160 μM, and stored in aliquots at −80 °C. crRNA and tracrRNA aliquots were thawed, mixed 1:1 by volume, and annealed by incubation at 37 °C for 30 min to form an 80 μM gRNA solution. Recombinant Cas9 was stored at 40 μM in 20 mM HEPES-KOH, pH 7.5, 150 mM KCl, 10% glycerol, 1 mM DTT, were then mixed 1:1 by volume with the 80 μM gRNA (2:1 gRNA to Cas9 molar ratio) at 37 °C for 15 min to form an RNP at 20 μM. RNPs were electroporated immediately after complexing. Human CD4+ T cells were prepared for electroporation as follows: human CD4+ T cells were collected from their culture vessels and centrifuged for 5 min at 300g, aspirated, and resuspended in the Lonza electroporation buffer P3 using 20 μl buffer per 200,000 cells. Two-hundred-thousand human CD4+ T cells were electroporated per well using a Lonza 4D 96-well electroporation system with pulse code EH115 (human). Immediately after electroporation, 80 μl of prewarmed medium was added to each well and the cells were incubated at 37 °C for 15 min. The cells were then transferred to a round-bottom 96-well tissue culture plate and cultured in 10% RPMI Medium, supplemented with 10% FBS, 50 μM 2-mercaptoethanol, 10uM N-acetyl l-cysteine and 1% penicillin/streptomycin with hIL-2 at 300 U ml−1 at 200,000 cells per well in 200 μl of medium. Guide primer sequences are as follows: sgSCR – GCGACTAGTACGCGTAGGTT, sgCXCR4 – TCTTTTACATCTGTGTTAGC, sgATF7ip#1

– GAGGCAGCATCACTAGAGGA, sgATF7ip#2 – ACTAGAGGCTATATCATCAG, sgATF7ip#3 – GGATGGCTCTGTAGAAGCTG.

Synthego Analysis -

Editing of the DNA was confirmed by Inference of CRISPR Edits (Synthego) analysis 4–8 days post-electroporation. A total of 5×10^4 cells were resuspended in 30 μl of QuickExtract DNA Quick Extraction solution (Epicentre) to lyse the cells and extract genomic DNA. The cell lysate was incubated at 65 °C for 15 min, 95 °C for 5 min, and then stored at −20 °C until PCR could be performed across the CRISPR–Cas9 target sites. Unique genomic primers to amplify across the proposed cut sites were designed using the Primer3 online web tool (http://bioinfo.ut.ee/primer3/), chemically synthesized (Integrated DNA Technologies), and suspended at 100μM. Each PCR reaction contained 2 μl 10× High-fidelity PCR buffer (Life Technologies), 3 μl 2 mM dNTPs (Bioline), 0.8 μl 50 mM MgCl2 (Life Technologies), 0.6 μl 10 μM forward primer, 0.6 μl 10μ M reverse primer, 0.2 μl 5 U μl−1 Platinum HIFI Taq (Life Technologies), 1 μl extracted DNA, and 11.8 μl H2O. The thermocycler setting consisted of one step at 95 °C for 5 min, followed by 14 cycles at 94 °C for 20 s, 65 °C for 20 s and 72 °C for 1 min (wherein the annealing temperature was decreased by 0.5 °C per cycle), followed by 35 cycles at 94 °C for 20 s, 58 °C for 20 s and 72 °C for 1 min with one final step at 72 °C for 10 min. PCR cleanup and capillary sequencing was performed by Sequetech (Mountain View, CA). Sequencing traces were analysed with the Synthego webtool (https://www.synthego.com/products/bioinformatics/crispr-analysis). Primer sequences are as follows: CXCR4 Fwd GTGCCCTTAGCCCACTACTTCA, CXCR4 Rev GGCCAACCATGATGTGCTGAAA, ATF7ip Fwd CGTCAGCAACTTGAAGCAGTGT, ATF7ip Rev TCATCAGAGGCCAGTTCACCAG.

Mixed Bone Marrow Chimera -

Bone marrow chimeras were generated by lethally irradiating 8-week-old recipient CD45.2 C57BL/6 mice with 550R gamma radiation for 2–5 minutes. Irradiation was repeated 3 hours later for a total dose of 1100R. C57BL/6 mice were reconstituted i.v. with equal amounts (5×10^6 cells) of bone marrow isolated from the long bones of CD451.2/*CD4*-Cre/*Atf7ip^{fl/fl}* and CD45.1/*CD4*-Cre*/Atf7ip^{+/fl}* mice. Bone marrow chimeras were reconstituted for 60 days prior to infection with 2×10^5 PFU LCMV Armstrong.

Flow cytometry and intracellular staining -

LN and spleen were isolated by dissection from mice and then mashed through a 70 um filter. Spleen cells were lysed in ammonium-chloride-potassium lysis buffer to remove red blood cells and were subsequently counted and plated in 96-well round bottom plates at a concentration of $1–5 \times 10^6$ cells per well. Cells were first stained with Ghost Dye (Tonbo), followed by blocking in 24G2 before staining with the appropriate antibodies for flow cytometry. For intracellular and transcription factor staining, cells were fixed overnight in the eBioscience Foxp3/Transcription Factor/Fixation-Concentrate kit (Thermo Fisher Scientific). After fixation, cells were permeabilized and stained with the appropriate antibodies. For intracellular cytokine staining, cells were stimulated for 4hrs with Brefeldin

A (eBioscience) and GP$_{33-41}$ peptide (1ug/ml). Cells were then fixed and permeabilized using the BD cytofix/cytoperm kit before staining with the appropriate antibodies.

Antibodies/tetramers used for flow cytometry were as follows: PE-Cy7-conjugated CD4 (clone RM4–5; Tonbo), PE-Cy7-conjugated CD62L (clone MEL-14; Tonbo), PE-Cy7-conjugated CD45 (clone 30-F11; Invitrogen), PE-Cy7-conjugated CD127 (clone A7R34; BioLegend), PE-conjugated IL-17A (clone eBio17B7; Invitrogen), PE-conjugated CD62L (clone MEL-14; Tonbo), PE-conjugated CD44 (clone IM7; BioLegend), PE-conjugated CD8 (clone 53–6.7; Tonbo), PE-conjugated RORγ (Q31–378; BD Biosciences), PE-conjugated TCF1/TCF7 (clone C63D9; Cell Signaling Technologies), PE-conjugated IL-13 (clone eBio13A; Invitrogen), PE-conjugated TNFa (clone MP6-X522; Invitrogen), PE-conjugated CD45.2 (clone 104; BioLegend), FITC-conjugated Thy1.2 (clone 53–2.1; BD Biosciences), FITC-conjugated IFNγ (clone xMG1.2; Invitrogen), FITC-conjugated Foxp3 (clone FJK-16s; Invitrogen), FITC-conjugated CD44 (clone IM7; BioLegend), FITC-conjugated CD8 (clone 53–6.7; Tonbo), FITC-conjugated CD19 (1D3; BD Biosciences), FITC-conjugated KLRG1 (clone 2F1; Southern Biotech), FITC-conjugated Granzyme B (clone QA16A02; BioLegend), A488-conjugated EOMES (clone Dan11mag; Invitrogen), allophycocyanin (APC)-conjugated Thy1.1 (clone OX-7; BioLegend), APC-conjugated CD25 (clone PC61.5; Tonbo), APC-conjugated CD4 (clone GK1.5; BioLegend), APC-conjugated IL-2 (clone JES6–5H4; Invitrogen), APC-conjugated CD62L (clone MEL-14; Tonbo), APC-conjugated CD45.1 (clone A20; BioLegend), APC-conjugated H-2Db-GP33–41 tetramer (NIH core facility), Alexa Fluor 647-conjugated Tbet (clone 4B10; BioLegend), APCCy7-conjugated CD45.1 (clone A20; BioLegend), PerCP-conjugated CD45 (clone 30-F11; Invitrogen), PerCPCy5.5-conjugated CD45.2 (clone 104; Tonbo), eFluor 450-conjugated TCRβ (clone H57–597; Tonbo), PerCP-Cy5.5-conjugated CD4 (clone GK1.5; BioLegend), BUV737-conjugated CD8a (clone 53–6.7; BD Biosciences), Ghost Dye (Tonbo), cell trace violet (Invitrogen)

ELISA –

Mouse CD8+ or human CD4+ T cells were stimulated for 24 hours in the presence of TCR stimulation (2ug anti-CD3) and costimulation (2ug anti-CD28) and supernatant was collected. IL-2 ELISA was performed using Ready-Set-Go ELISA Kits (eBioscience).

RNA isolation and qPCR -

RNA was isolated using the RNeasy micro kit (Qiagen). Isolated RNA was reversed transcribed using superscript IV reverse transcription (Invitrogen) with OligoDT20 primers (Invitrogen). qPCR was performed on the Applied Biosystems QuantStudio3 machine using Quantabio Perfecta qPCR ToughMix Low Rox. All reactions were normalized to *Actin* (*ActB*), and fold induction was calculated using the ddCT method. All primer-probes were purchased from ABI: *Il7r* (FAM-MGB) Mm00434295_m1, *Eomes* (FAM-MGB) Mm01351985_m1, *Sell* (FAM-MGB) Mm00441291_m1, *Atf7ip* (FAM-MGB) Mm00479827_m1, *ActB* (FAM-MGB) Mm00607939_s1, *IL2* (FAM-MGB) Hs00174114_m1, and *GAPDH* (FAM-MGB) HS03929097. LCMV viral load was quantitated using qPCR as performed by (32). Briefly, 5mg of Liver or Spleen was homogenized in Trizol prior to total RNA isolation. cDNA synthesis was performed

with superscript IV reverse transcriptase (Invitrogen) using LCMV specific primers. qPCR was performed with SYBR green (Applied Biosystems) using the following LCMV specific primers to the GP gene: GP-R (GCAACTGCTGT-GTTCCCGAAAC) and GP-F (CATTCACCTGGACTTTGTCA-GACTC). Repeat elements were quantified as described previously using major satellite DNA repeats and LINE primers (33). Total RNA was extracted as above, and cDNA was made using random hexamers and oligo dT in 1:4 ratio as recommended by the manufacturer (Verso cDNA synthesis kit, ThermoFisher). Repeats were then quantified using SYBR green PCR master mix (Applied Bioscience) on the Applied Biosystems QuantStudio3 machine. Primers for major repeats, Forward primer: 5' – GACGACTTGAAAAATGACGAAATC-3', Reverse primer: 5'-CATATTCCAGGTCCTTCAGTGTGC-3'. Primers for LINE elements, Forward primer: 5'- TTTGGGACACAATGAAAGCA-3', Reverse primer: 5' – CTGCCGTCTACTCCTCTTGG-3'

RNA-seq -

Total RNA was extracted using Trizol and purified using a Qiagen microcolumn. Illumina libraries were generated from total RNA using the Illumina TruSeq Library Prep Kit and sequenced on the Illumina HiSeq 4000 to a depth of 20 million reads. Sequence alignment was performed using STAR (version 2.7.9a; (34)). Mappings were restricted to those that were uniquely assigned to the mouse genome, and unique read alignments were used to quantify expression and aggregated on a per-gene basis using the Ensembl (GRCm39) annotation. Differentially expressed genes between experimental groups were then determined using DESeq2 (V4.0.3; (35)). Retroelement expression was analyzed using TEtranscripts (36). Alignment was performed with recommended specifications for repeat regions using STAR (version 2.7.9a; (34)). The bam files thus generated were used for TE-transcript version 2.0.3 along with mouse specific TE GTF files. Differentially expressed repeats were determined using DEseq2 as above.

ChIP -

ChIP was performed by Active Motif. Primary naive T cells were fixed with 1% formaldehyde for 15 min and quenched with 0.125 M glycine. Chromatin was isolated by the addition of lysis buffer, followed by disruption with a Dounce homogenizer. Lysates were sonicated, and the DNA was sheared to an average length of 300–500 bp. Genomic DNA (input) was prepared by treating aliquots of chromatin with RNase, proteinase K, and heat for de-cross-linking, followed by ethanol precipitation. Pellets were resuspended, and the resulting DNA was quantified on a NanoDrop spectrophotometer. Extrapolation to the original chromatin volume allowed quantitation of the total chromatin yield. An aliquot of chromatin (15 μg) was precleared with protein A agarose beads (Invitrogen). Genomic DNA regions of interest were isolated using 5 μg of antibody against H3K9me3 (Active Motif). Complexes were washed, eluted from the beads with SDS buffer, and subjected to RNase and proteinase K treatment. Cross-links were reversed by incubation overnight at 65°C, and ChIP DNA was purified by phenol-chloroform extraction and ethanol precipitation. The quality of ChIP-isolated DNA was tested by qPCR. qPCR reactions were performed in triplicate on specific genomic regions using SYBR Green Supermix (Applied Biosystems).

The resulting signals were normalized for primer efficiency by carrying out qPCR for each primer pair using input DNA.

ChIP-seq -

ChIP-seq and subsequent data analysis was performed by Active Motif. Illumina sequencing libraries were prepared from the ChIP and input DNAs by the standard consecutive enzymatic steps of end-polishing, dA-addition, and adaptor ligation. After a final PCR amplification step, the resulting DNA libraries were quantified and sequenced on Illumina's NextSeq 500 (75-nt reads, single end). Reads were aligned to the mouse genome (mm10) using the Burrows-Wheeler Aligner algorithm (default settings[37]). Duplicate reads were removed, and only uniquely mapped reads (mapping quality 25) were used for further analysis. Alignments were extended in silico at their 3′ ends to a length of 200 bp, which is the average genomic fragment length in the size-selected library, and assigned to 32-nt bins along the genome. The resulting histograms (genomic "signal maps") were stored in bigWig files. H3K9me3-enriched regions were identified using the Spatial Clustering for Identification of ChIP-Enriched Regions algorithm (spatial clustering for identification of ChIP-enriched regions; [38]) at a cutoff of FDR 1×10^{-10} and a max gap parameter of 600 bp. Peaks that were on the ENCODE (Encyclopedia of DNA Elements) blacklist of known false ChIP-seq peaks were removed. Signal maps and peak locations were used as input data to the Active Motifs proprietary analysis program, which creates Excel tables containing detailed information on sample comparison, peak metrics, peak locations, and gene annotations.

Western blot -

Extracts for Western blotting were isolated as previously performed [16]. Five million $CD8^+$ T cells were lysed in cytoplasmic buffer containing 10 mM Hepes, 1.5 mM $MgCl_2$, 10 mM KCl, 0.5 mM dithiothreitol, EDTA-free protease inhibitor cocktail, and 0.1% IGEPAL. The nuclear pellet was isolated by centrifugation at 1,500 rpm for 5 min. The total nuclear extract was isolated by incubation of the nuclear pellet with 1% SDS and 1:100 benzonase. The nuclear extract was heated in sample buffer containing SDS for 10 min at 70°C before separation with SDS-PAGE and transfer to a polyvinylidene fluoride membrane. The membrane was then blocked with 5% milk in TBST (Tris-buffered saline and Tween 20) followed by overnight incubation with the primary antibody. The membrane was washed 4× for 5 min in Tris-buffered saline and Tween 20 before incubation in HRP-conjugated secondary antibody. The membrane was visualized with ECL reagent (Thermo Fisher Scientific). Antibodies used for Western blot were as follows: anti-MACF1 (ab84497; Abcam); Anti-LaminB1, Nuclear Loading Control (ab65986; Abcam); peroxidase affinipure goat anti-rabbit IgG (H+L; 111-035-144; Jackson ImmunoResearch).

ChIP qPCR -

7×10^6 naive T cells were used for each ChIP reaction following the protocol from the Diagenode LowCell# Chip Kit protein G. Briefly, cells were lysed and then sonicated for 5 min using a Covaris s220 sonicator. ChIP was performed using an H3K9me3 antibody from Abcam (ab8898) and an irrelevant IgG control (Diagenode C15410206). qPCR was performed using SYBR green (Applied Biosystems) with the following primer pairs: *Il2/*

Il21: forward, 5′-GGGGCAGTAACTTCGACTTG-3′, and reverse, 5′-AGTCGAGCTGAG ATGTGGAA-3′; and *Il7r*: forward, 5′- GGCCAGCATTTGTGTTCTCT-3′, and reverse, 5′- TTATACCAGCTTTCCCGCCA-3′. The primer concentration per 25-μl qPCR reaction was 200 nM. 5 μl of ChIP-isolated DNA was used per reaction. Relative Ct values obtained were normalized against the total input to obtain the percentage of amplified ChIP DNA per input.

Statistical analysis -

All experiments were performed using randomly assigned mice without investigator blinding. No data were excluded. Statistical significance between two groups was calculated using an unpaired, parametric, two-tailed Student's *t* test or the nonparametric Mann–Whitney test. Experimental groups included a minimum of three biological replicates. Intragroup variation was not assessed. All statistical analysis was performed using Prism 7 (GraphPad Software). Figures display means ± SD unless noted otherwise. A P value <0.05 was considered statistically significant. No statistical methods were used to predetermine sample size.

Results:

Deletion of ATF7ip in T cells enhances CD8+ T cell effector function

We hypothesized that ATF7ip may have a function in CD8+ T cells secondary to the significant expression of *Atf7ip* mRNA in CD8+ T cells in public RNA expression databases (Immgen) (Fig. 1A). Within CD8+ T cell subsets, *Atf7ip* was highly expressed in naïve T cells (CD62L+CD44-) with lower expression in central memory (CM) (CD62L+CD44+) and in effector-memory CD8+ T cells (EM) (CD62L-CD44+) (Fig. 1B). Prior work in CD4+ T cells showed decreased *Atf7ip* expression with CD4+ T cell stimulation(30). Activation of the T cell receptor (TCR) of naïve CD8+ T cells (CD62L+CD44-) with anti-CD3 antibodies in combination with co-stimulation of the CD28 co-receptor for the TCR caused a decrease in *Atf7ip* mRNA expression (Fig. 1C), suggesting that, similar to CD4+ T cells(30), the release of negatively regulated targets of ATF7ip may be important in CD8+ T cell activation and action. Moreover, *Atf7ip* mRNA levels decreased within effector CD8+ T cells after LCMV infection further suggesting that CD8+ T cell activation by a pathogen decreased *Atf7ip* expression. (Fig. 1A).

To interrogate the potential *in vivo* function of ATF7ip in CD8+ T cells, a conditional deletion allele of mouse *Atf7ip* was utilized that contained a targeting construct surrounding exon 2 of *Atf7ip* with loxP Cre-recombination sites (*Atf7ip*^fl/fl mice)(30). In the presence of Cre-recombinase, loxP-directed recombination will result in the deletion of exon 2 and removal of the start codon and an out-of-frame mRNA transcript containing a premature stop codon. To examine the function of ATF7ip in T cells, *Atf7ip*^fl/fl mice were crossed to transgenic mice expressing Cre recombinase from the CD4 promoter (*CD4*-Cre). Because the *CD4*-cre transgene is expressed at the double-positive stage of thymic T cell development it will delete ATF7ip in both CD4+ and CD8+ T cells. Quantitative polymerase chain reaction (qPCR) using primers specific for exon 2 of *Atf7ip* confirmed the deletion of *Atf7ip* mRNA in CD8+ T cells (Supplemental Fig. 1A) and western blot confirmed deletion of ATF7ip protein (Supplemental Fig. 1B). Extensive immune profiling in both *CD4*-Cre/

Atf7ip^{+/fl} T cells and *CD4*-Cre*/Atf7ip*^{fl/fl} T cells indicated no differences in steady-state lymph node (Supplemental Fig.1C)/spleen (**data not shown**) naïve, CM, or EM T cells.

To assess the effect of T cell specific deletion of *Atf7ip* on CD8+ T cell effector function, we infected cohorts of *CD4*-Cre/*Atf7ip*^{+/fl} mice and *CD4*-Cre/*Atf7ip*^{fl/fl} mice with either Listeria Monocytogenes (LM) or lymphocytic choriomeningitis (LCMV) Armstrong strain and monitored bacterial and viral load, respectively. Both of these infections are known to stimulate a robust CD8+ T cell response(39). Notably, *CD4*-Cre/*Atf7ip*^{fl/fl} mice had significantly decreased bacterial burden after lethal LM infections (Fig. 1D) and reduced LCMV viral load by quantitative PCR (qPCR) (32)(Supplemental Fig.1D). In the lethal LM infection, *CD4*-Cre/*Atf7ip*^{+/fl} mice were euthanized at day 6 secondary to weight loss and poor appearance (Fig. 1D) while *CD4*-Cre/*Atf7ip*^{fl/fl} mice lost minimal weight and appeared healthy suggesting that they were better able to clear the LM infection. To better characterize the cellular phenotype of CD8+ T from *CD4*-Cre/*Atf7ip*^{+/fl} mice and *CD4*-Cre/ *Atf7ip*^{fl/fl} mice, we infected cohorts of mice with LCMV and monitored virus specific T cells using an H2D^b MHC Class I tetramer containing the GP$_{33-41}$ epitope of LCMV. We did not find a difference in the percentage or absolute number of GP33 specific CD8+ T cells nor did we find a difference in effector cytokine production (Supplemental Fig.1E and 1F). We did appreciate a skewing toward a CD8+ memory precursor phenotype in the spleen (Supplemental Fig.1G) in *CD4*-Cre/*Atf7ip*^{fl/fl} mice as evidenced by increased IL7r expression (CD127).

To determine if there were global changes in gene expression in *Atf7ip*-deficient CD8+ T cells that could contribute to their increased effector function, we performed RNA-Seq. LCMV specific CD8+ T cells were isolated by flow cytometry from LCMV infected *CD4*-Cre/*Atf7ip*^{+/fl} and *CD4*-Cre/*Atf7ip*^{fl/fl} mice and tetramer positive cells sent for RNA-seq analysis. There were a large number of differently expressed genes within CD8+ T cells with 1007 genes upregulated in *CD4*-Cre/*Atf7ip*^{fl/fl} CD8+ T cells (FDR<0.01, log2fold >0.75) and 607 upregulated genes in *CD4*-Cre/*Atf7ip*^{+/fl} CD8+ T cells (FDR<0.01, log2fold >0.75) (Fig. 1E). As expected, there were more genes upregulated in *Atf7ip*^{fl/fl} CD8+ T cells consistent with deletion of a repressive histone mark. **Kyoto Encyclopedia of Genes and Genomes (KEGG)** analysis revealed that the top pathways of upregulated genes in *Atf7ip*^{fl/fl} CD8+ T cells involved DNA replication and metabolism while the modules of upregulated genes in *Atf7ip*^{+/fl} CD8+ T cells were associated with T cell signaling (Supplemental Fig.1H). Based on the KEGG analysis, *Atf7ip*^{fl/fl} CD8+ T cells appear to be metabolically active. Moreover, *Atf7ip*^{fl/fl} CD8+ T cells were transcribing significantly more CD8+ T cell effector molecules such as granzymes (*Gzmb, Gzmk, Gzmm*). Consistent with our flow data (Supplemental Fig.1G), *Atf7ip*^{fl/fl} CD8+ T cells had increased *Il7r* expression although it did not meet the FDR 0.01 significance cutoff (data not shown). Altogether, the RNA-seq data are consistent with *Atf7ip*^{fl/fl} CD8+ T cells appearing highly activated with increased *IL7r* expression.

Our data shows that CD8+ T cells are more activated in *CD4*-Cre/*Atf7ip*^{fl/fl} mice after infection and that these mice are more resistant to primary infections with both LM and LCMV. We next sought to determine if *CD4*-Cre/*Atf7ip*^{fl/fl} mice had altered memory responses. To test the role of ATF7ip in the memory response, we performed a primary

infection of *CD4*-Cre/*Atf7ip*$^{+/fl}$ mice and *CD4*-Cre/*Atf7ip*$^{fl/fl}$ mice with LCMV and then a secondary infection (> 60 days later) with a strain of LM that expresses the LCMV H2D^b restricted GP$_{33–41}$ epitope (LM33) (Fig. 1F). This experimental system has been widely used to evaluate CD8+ memory responses(13). Notably, *CD4*-Cre/*Atf7ip*$^{fl/fl}$ mice have improved memory responses and similar to primary infections with LCMV, activated *Atf7ip*$^{fl/fl}$ CD8+ memory T cells produce increased granzyme B (Fig. 1G) without changes in the number of GP33-specific CD8+ T cells, or effector cytokine production (Supplemental Fig.1I). As granzyme B is a critical cytotoxic molecule for clearance of infectious organisms, increased levels could explain the heightened primary and secondary responses in *CD4*-Cre/*Atf7ip*$^{fl/fl}$ mice.

One caveat to these studies showing increased effector function in *CD4*-Cre/*Atf7ip*$^{fl/fl}$ mice, is that deletion of *Atf7ip* is not CD8+ T cell intrinsic as both CD4+ and CD8+ T cells will have deletion of *Atf7ip*. As CD4+ T cells can provide help to CD8+ T cell function, deletion of *Atf7ip* in CD4+ T cells may contribute to increased CD8+ T cell effector function. Our previous work has shown that deletion of *Atf7ip* in CD4+ T cells results in enhanced IL-2 production with TCR stimulation. IL-2 has previously been shown to enhance CD8+ T cell effector function and granzyme production(40–43); thus IL-2 from CD4+ T cells may be the cause of enhanced clearance of infections. To determine if increased IL-2 contributes to enhanced effector function, we infected mice with a lethal dose of LM-33 in the presence of blocking antibodies to IL-2 (S4B6) or isotype control. As expected, isotype treated *CD4*-Cre/*Atf7ip*$^{fl/fl}$ mice had reduced bacterial load compared to isotype treated *CD4*-Cre/*Atf7ip*$^{+/fl}$ mice (Fig. 1H). Remarkably, treatment with S4B6 completely blocked the reduced bacterial load seen in *CD4*-Cre/*Atf7ip*$^{fl/fl}$ mice and these mice had a similar bacterial burden as *CD4*-Cre/*Atf7ip*$^{+/fl}$ mice treated with S4B6. In addition, S4B6 treated mice had enhanced weight loss and the experiment had to be stopped at day 5 secondary to the poor appearance of S4B6 treated mice. As expected, GP33+CD8+ T cells from isotype treated *CD4*-Cre/*Atf7ip*$^{fl/fl}$ mice showed enhanced granzyme B production compared to GP33+ CD8+ T cells from isotype treated *CD4*-Cre/*Atf7ip*$^{+/fl}$ mice (Fig. 1I). The difference in granzyme B production was abolished with S4B6 treatment suggesting that enhanced IL-2 production in T cells with *Atf7ip*-deletion is responsible for increased granzyme B production. These results indicate that increased IL-2 production from T cells is the cause of enhanced protection in *CD4*-Cre/*Atf7ip*$^{fl/fl}$ mice from lethal LM infection.

Deletion of ATF7ip results in a T cell intrinsic enhancement of IL7r expression and CD8+ T cell memory

Deletion of *Atf7ip* in T cells results in enhanced effector function and the enhanced effector function may be due to both CD8+ T cell intrinsic effects as well as trans effects from increased IL-2 production in CD4+ T cells. We first assessed if *Atf7ip*-deletion in CD8+ T cells resulted in cell-intrinsic defects in proliferation by labeling naïve CD8+ T cells with cell-trace violet (CTV) and then activating them in vitro with anti-CD3 and anti-CD28 for 24 and 48 hours. CTV experiments revealed similar in vitro proliferation of naïve CD8+ T cells from *CD4*-Cre/*Atf7ip*$^{+/fl}$ and *CD4*-Cre/*Atf7ip*$^{fl/fl}$ mice at 24hrs with a modest increase in proliferation at 48hrs (Supplemental Fig. 2A). In order to gain insight into CD8+ T cell intrinsic alterations in gene regulation, global gene expression analysis was performed

on naive CD8+ T cells and naïve CD8+ T cells activated *in vitro* with anti-CD3 and anti-CD28 for 24 hours. Principal component analysis (PCA) yielded clustering of the samples (Supplemental Fig.2B). A previous study of *ATF7ip* deletion in HeLa cells and our studies of *Atf7ip*-deletion in CD4+ T cells implicated ATF7ip in silencing ZFPs (16). In line with these studies, *Atf7ip*-deletion in naïve CD8+ T cells resulted in the overexpression of several ZFPs such as *Zfp53*. (Fig. 2A). Interestingly, at 24 hours of CD3/CD28 stimulation *Atf7ip*-deletion in CD8+ T cells resulted in increased mRNA expression of markers of CD8+ T cell memory such as *Il7r, Eomes*, and *Sell* (Fig. 2A). Il7r has previously been shown to mark CD8+ memory cells and in an acute infection Il7r positive cells will populate the CD8+ memory population that will serve as the reservoir to guard against repeat infection with the same microorganism(5). Eomes is a transcriptional factor that is critical for CD8+ memory formation(7). Thus, increased expression of both *Il7r* and *Eomes* suggested that *Atf7ip*-deletion in CD8+ T cells may enhance their memory potential. We confirmed the transcriptional changes seen in the RNA-seq data by performing qPCR for *Il7r, Eomes*, and *Sell* on naïve CD8+ T cells from *CD4*-Cre/*Atf7ip*$^{+/fl}$ mice and *CD4*-Cre/*Atf7ip*$^{fl/fl}$ mice after CD3/CD28 stimulation for 24 and 48hrs (Fig. 2B and 2C). RNA-seq data showing increased *Il7r* expression is consistent with our data showing increased Il7r expression on CD8+ T cells from *CD4*-Cre/*Atf7ip*$^{fl/fl}$ after LCMV infection (Supplemental Fig.1G).

We next sought to determine if these transcriptional changes also correlated with CD8+ T cell intrinsic altered protein production. To determine if the phenotypic changes observed in *Atf7ip*-deficient CD8+ T cells occur in a cell- intrinsic manner, we utilized the CD8+ P14 TCR transgenic mouse line that recognizes the GP33 epitope of LCMV. We crossed P14 transgenic mice to *CD4*-Cre/*Atf7ip*$^{fl/fl}$ mice and co-transferred equal numbers of P14+/CD45.1/*Atf7ip*$^{+/fl}$ CD8+ T cells and P14+/CD45.1.2/*Atf7ip*$^{fl/fl}$ CD8+ T cells into CD45.2 C57Bl/6 hosts prior to LCMV infection (Fig. 2D). We followed the transfer experiment over time and analyzed splenocytes at day 8, day 15, and day 60. The day 8 timepoint was chosen as it is the peak of terminal effector formation after LCMV infection and by day 60 the majority of P14+ cells should be memory cells. Day 15 was chosen as an intermediate timepoint. Notably, P14+/CD45.1.2/*Atf7ip*$^{fl/fl}$ CD8+ T cells have increased expression of the IL7r (CD127) at day 8, day 15, and day 60 and decreased expression of KLRG1 indicating a cell-intrinsic effect on CD8+ memory formation (Fig. 2E and 2F). To further probe if *Atf7ip*-deletion in CD8+ T cells results in increased Il7r expression, we performed mixed bone-marrow (BM) chimera studies by isolating bone marrow from *CD4*-Cre/*Atf7ip*$^{+/fl}$ mice and *CD4*-Cre/*Atf7ip*$^{fl/fl}$ mice with distinct congenic markers and transplanting the marrow into lethally irradiated B6 hosts. Mixed BM chimera studies showed an increase in Il7r expression with *Atf7ip*-deletion in CD8+ T cells after LCMV infection (Supplemental Fig. 2C).

While *Atf7ip*-deletion in CD8+ T cells results in a cell-intrinsic increase in IL7r expression, we next wanted to confirm that these cells displayed characteristics of CD8+ T cell memory. A significant amount of work has characterized the transcription factors associated with terminal effector and memory precursor formation. The transcription factor TCF-1 has been shown to have increased expression CD8+ memory cells and to be required for their induction and maintenance. Deletion of TCF-1 results in an attenuated memory response to infection and TCF-1 acts by inducing the memory associated transcription factor

Eomes(8). Whereas TCF-1 is critical for CD8+ memory, TBET is required for terminal effector formation and the clearance of pathogens during an infection(6). We analyzed TCF-1 and TBET expression at day 60 of the P14 transfer experiment and found that P14+/CD45.1.2/*Atf7ip*^(fl/fl) CD8+ T cells had significantly more TCF-1 expression and reduced TBET expression when compared P14+/CD45.1/*Atf7ip*^(+/fl) CD8+ T cells (Fig. 2G and 2H). Enhanced TCF-1 expression is consistent with increased Il7r expression and suggests that *Atf7ip*-deletion in CD8+ T cells results in increased numbers of transcriptionally active memory cells.

To further characterize cell-intrinsic changes in CD8+ T cells with *Atf7ip*-deletion, we measured intracellular cytokine levels in P14+/CD45.1.2/*Atf7ip*^(fl/fl) CD8+ T cells and P14+/CD45.1/*Atf7ip*^(+/fl) CD8+ T cells isolated at early and late time points. At Day 8 we did not appreciate a difference in IL-2, IFNγ, or TNFα after *in vitro* stimulation with GP33 peptide (Supplemental Fig.2D). Similarly, mixed BM chimera studies did not show altered cytokine production at day 8 (**data not shown**). Consistent with prior studies showing CD8+ memory cells produce increased IL-2 after stimulation(44), both P14+/CD45.1.2/*Atf7ip*^(fl/fl) CD8+ T cells and P14+/CD45.1/*Atf7ip*^(+/fl) CD8+ T cells had an increased percentage of IL-2 producing cells at day 60 when compared to day 8 (Fig. 2I, Supplemental Fig.2D). Interestingly, P14+/CD45.1.2/*Atf7ip*^(fl/fl) CD8+ T had a higher percentage of IL-2/IFNγ+ producing cells compared to P14+/CD45.1/*Atf7ip*^(+/fl) CD8+ T cells. This result suggests that IL-2 may be dysregulated in CD8+ T cells similar to CD4+ cells with deletion of *Atf7ip* resulting in enhanced production of this cytokine in both CD4+ and CD8+ T cells. The function of autocrine IL-2 in CD8+ T cells is controversial as CD4+ T cells produce much higher levels with activation and are thought to be the primary source of IL-2 during an infection. Recent studies have shown that CD8+ autocrine IL-2 is important for CD8+ memory responses with *Il2*-deficient CD8+ memory cells showing reduced proliferative capacity after repeat infection and reduced memory formation(45–47). Because *Atf7ip*-deletion results in increased numbers of memory cells that produce increased IL-2, we hypothesized that *Atf7ip*^(fl/fl) CD8+ T cells may have a CD8+ T cell intrinsic enhancement of the memory response. To address this question, we performed the following two experiments. First, we transferred P14+/CD45.1/*Atf7ip*^(+/fl) CD8+ T cells and P14+/CD45.1.2/*Atf7ip*^(fl/fl) CD8+ T cells into individual mice and then utilized a similar experimental set-up as performed in Figure 1F with a primary LCMV infection followed by a secondary infection with LM33 (Supplemental Fig.2E). Second, we co-transferred both P14+/CD45.1.2/*Atf7ip*^(fl/fl) CD8+ T cells and P14+/CD45.1/*Atf7ip*^(+/fl) CD8+ T cells into B6 hosts, infected the mice with LCMV and waited > 60 days prior to flow sorting T cells based on congenic markers CD45.1/CD45.1.2. Equal numbers of either CD45.1 or CD451.2 memory T cells were then injected IV into individual naïve B6 hosts prior to infection with LM-33 (Supplemental Fig.2F). In either experimental set-up, transfer of P14+/CD45.1.2/*Atf7ip*^(fl/fl) CD8+ T cells lead to an augmented memory response as shown by reduced LM found in both the liver and spleen (Fig. 2J and 2K). Moreover, *Atf7ip*-deletion resulted in increased clonal expansion or survival of memory cells as evidenced by increased abundance of P14+/CD45.1.2/*Atf7ip*^(fl/fl) CD8+ T cells. This may be consistent with increased autocrine IL-2 driving augmented expansion or survival. These results indicate that *Atf7ip*-deletion results in a CD8+ T cell intrinsic enhancement of the memory response which could be due

to both increased numbers of memory cells and enhanced function through increased IL-2 production.

ATF7ip is required for H3K9me3 deposition at the *Il7r* locus and *Il2* locus in CD8+ T cells

We next turned to the mechanism by which ATF7ip regulates CD8+ T cell memory. As outlined earlier, the most well characterized function of ATF7ip is to help promote the generation of the repressive H3K9me3 histone mark in chromatin. Prior work has shown that in naïve CD4+ T cells ATF7ip silences *Il2* gene expression through deposition of H3K9me3 in the *Il2-Il21* intergenic region. Thus, deletion of *Atf7ip* results in less repression of the *Il2* locus and increased IL-2 production with TCR stimulation in CD4+ T cells(30). We hypothesized that similar mechanisms would act in naïve CD8+ T cells so we performed ChIP-seq on naïve CD8+ T cells using an antibody directed to the H3K9me3 mark. H3K9me3 ChIP-seq was performed in duplicate on naïve CD8+ T cells from both *CD4*-Cre/*Atf7ip^{+/fl}* mice (*Atf7ip^{+/fl}* naïve CD8+ T cells) and *CD4*-Cre/*Atf7ip^{fl/fl}* mice (*Atf7ip^{fl/fl}* naïve CD8+ T cells) and yielded approximately 52,020 H3K9me3 active sites in both genotypes. Peak size boxplots were created for each of the ChIP-seq samples and showed similar tag numbers indicating that there was not a profound reduction of H3K9me3 with *Atf7ip*-deletion in naïve CD8+ T cells (Fig. 3A). Moreover, there was a high correlation in tag numbers between samples (Supplemental Fig.3A).

Although there was not a difference in H3K9me3, hierarchical clustering showed that the samples clustered by genotype (Fig. 3B). Interestingly, there were 251 sites with a two-fold increase in H3K9me3 deposition in *Atf7ip^{+/fl}* naïve CD8+ T cells compared to *Atf7ip^{fl/fl}* naïve CD8+ T cells while there were only 38 sites with a twofold increase in *Atf7ip^{fl/fl}* naïve CD8+ T cells (Fig. 3C). These results support a role for ATF7ip in promoting the formation of the H3K9me3 mark at specific genomic locations in naïve CD8+ T cells. Consistent with prior work in HeLa cells, a large number of zinc finger genes had a significant decrease in H3K9me3 in *Atf7ip^{fl/fl}* naïve CD8+ T cells relative to *Atf7ip^{+/fl}* naïve CD8+ T cells (Fig. 3C). Moreover, there were two sites of H3K9me3 deposition of approximately 3,399bp and 2,999bp and on chromosome 15 with a two-fold decrease of H3K9me3. These sites are downstream of the *Il7r* gene and ChIP-seq tracings showed a reduction of the H3K9me3 histone mark in this region (Fig. 3D) and H3K9me3 ChIP qPCR confirmed that there was less H3K9me3 downstream of the *Il7r* gene in *Atf7ip^{fl/fl}* naïve CD8+ T cells (Fig. 3E). Decreased H3K9me3 at the *Il7r* locus in *Atf7ip^{fl/fl}* naïve CD8+ T cells may result in less repression of the *Il7r* locus and increased *Il7r* expression in *Atf7ip^{fl/fl}* naïve CD8+ T cells after stimulation as well as increased *Il7r* expression with LCMV infection. Thus, aberrant *Il7r* expression may explain the increased number of memory cells in *Atf7ip^{fl/fl}* CD8+ T cells after infection. In addition to decreased H3K9me3 at the *Il7r* locus, there were multiple other immune effector genes with reduced H3K9me3 deposition in *Atf7ip^{fl/fl}* naïve CD8+ T cells such as *Zap70* and *Runx3* (Fig. 3F and 3G). Zap-70 is required for effective T cell activation after TCR stimulation and Runx3 has been shown to have multiple functions in CD8+ T cells including effector molecule production, memory precursor formation, tissue-resident memory formation, and the suppression of aberrant T follicular helper cell responses (TfH)(48–52). While there is reduced H3K9me3 at *Runx3* and *Zap70*, we have been unable to document changes in gene or protein expression of these

molecules and further studies are underway evaluating the role of dysregulated Runx3 and Zap70 in *Atf7ip^{fl/fl}* naïve CD8+ T cells.

H3K9me3 ChIP-seq data in *Atf7ip^{fl/fl}* naïve CD8+ T cells revealed a significant reduction of H3K9me3 at the *Il7r* locus which could explain increased *Il7r* expression. CD8+ T memory cells also show increased IL-2 expression (Fig. 2I) with *Atf7ip*-deletion so we hypothesized that H3K9me3 would also be reduced in *Atf7ip^{fl/fl}* naïve CD8+ T cells similar to *Atf7ip^{fl/fl}* naïve CD4+ T cells. Notably, analysis of ChIP-seq tracings in the *Il2-Il21* intergenic region of *Atf7ip^{fl/fl}* naïve CD8+ T cells showed decreased H3K9me3 deposition (Fig. 4A). This site was not decreased by greater than two-fold as we reported with *Atf7ip*-deletion in naïve CD4+ T cells(30), however, ChIP-seq tracings in naïve CD8+ T cells show a clear decrease in H3K9me3. This data suggested that *Atf7ip^{fl/fl}* naïve CD8+ T cells, similar to *Atf7ip^{fl/fl}* naïve CD4+ T cells, were similarly pre-primed to produce increased IL-2. ChIP-qPCR confirmed a reduction of H3K9me3 at the *Il2* locus in *Atf7ip^{fl/fl}* naïve CD8+ T cells (Fig. 4B). Moreover, stimulation of *Atf7ip^{fl/fl}* naïve CD8+ T cells with anti-CD3 and anti-CD28 resulted in increased IL-2 secretion compared to *Atf7ip^{+/fl}* naïve T cells (Fig. 4C). Consistent with prior studies, the magnitude of IL-2 produced by CD8+ T cells was significantly less than CD4+(53). Altogether, our data support a role for ATF7ip regulating H3K9me3 deposition at the *Il2* locus.

The finding that ATF7ip controlled H3K9me3 deposition at the *Il2* locus in CD4+ and CD8+ T cells suggested that there may be other shared loci that are targets for H3K9me3 deposition by ATF7ip. Indeed, further analysis of our ChIP-seq data from naïve CD4+ and naïve CD8+ T cells, revealed that there is substantial overlap in genomic sites targeted for H3K9me3 deposition by ATF7ip in CD4+ and CD8+ T cells with approximately 1/3 of the sites shared in naïve CD8+ T cells and naive CD4+ T cells (Fig. 4D). Consistent with the overlap, ChIP-seq tracings show similar decreases in H3K9me3 in *Atf7ip^{fl/fl}* naïve CD4+ T cells and *Atf7ip^{fl/fl}* naïve CD8+ T cells at the *Il7r* locus, *Zap70* locus, and *Runx3* locus (Fig. 4E, Supplemental Fig.3B and 3C). Furthermore, there were multiple ZFPs that showed decreased H3K9me3 in *Atf7ip^{fl/fl}* naïve CD4+ T cells and *Atf7ip^{fl/fl}* naïve CD8+ T cells (Fig. 4F). Collectively, the significant overlap in sites of H3K9me3 deposition regulated by ATF7ip suggested a shared mechanism of action for ATF7ip in both CD4+ and CD8+ T cells.

ATF7ip targets transposable elements for H3K9me3 deposition

To further explore why ATF7ip is driving H3K9me3 deposition at specific sites in CD4+ and CD8+ T cells, we examined the underlying nucleotide sequences at the genomic locations of ATF7ip dependent H3K9me3 deposition. Analysis of the 1199 bp sequence of H3K9me3 (green box Fig. 4A) within the *Il2/Il21* intergenic region revealed that approximately 82% of the sequence consisted of transposable elements (TE) as shown by Repeatmasker (http://www.repeatmasker.org) (Fig. 5A). Similarly, analysis of the regions of the ATF7ip dependent H3K9me3 deposition in the *Il7r* locus showed that the region contained approximately 94% TE (Supplemental Fig.3D). Global analysis of the genomic locations of ATF7ip H3K9me3 deposition revealed that they are enriched in TE in both CD4+ and CD8+ T cells with 96.4% of the ATF7ip dependent sites enriched in TE in

CD4+ T cells and 98% of the sites enriched in CD8+ T cells (Fig. 5B and 5C). Moreover, sites of ATF7ip-dependent H3K9me3 deposition largely consisted of Class I retroelements (Supplemental Fig.3E). These data argue that ATF7ip is targeting TE in CD4+ and CD8+ T cells for H3K9me3 deposition.

Consistent with ATF7ip's function in silencing TE, analysis of our RNA-seq data in CD8+ T cells shows increased expression of TE with deletion of *Atf7ip* using the TE transcripts algorithm, an algorithm that allows the analysis of highly repetitive TE that are often discarded during traditional RNA-seq analysis(36) (Fig. 5D–5F). Deletion of *Atf7ip* resulted in increased expression of TE in naïve CD8+ T cells and with CD8+ T cell activation *in vitro* or with LCMV. The TE that had the highest expression were Class I TE consisting mostly of ERV and LINE elements. We have previously performed RNA-seq on CD4+ T cells from *CD4*-Cre/*Atf7ip*^fl/fl^ mice(30). Both naïve *Atf7ip*^fl/fl^ CD4 T cells and naïve CD4+ T cells stimulated for 24hrs using *in vitro* Th17 inducing conditions showed increased TE expression (Fig. 5G and 5H). Notably, the ERV found in the *Il7r* locus (IAPEz-int) increased with cell stimulation suggesting de-repression of this loci with *Atf7ip* deletion. To confirm the RNA-seq results, we performed qPCR for TE elements and confirmed that TE expression was increased in CD8+ T cells (Fig. 5I). Altogether, our data shows that ATF7ip-dependent H3K9me3 deposition primarily targets TE in CD4+ and CD8+ T cells and that failure to silence these elements results in the aberrant expression of both TE and genes adjacent to TE such as *Il2* and *Il7r*.

Our data shows that ATF7ip is critical for silencing TE and inhibiting *Il2* gene expression in murine CD4+ and CD8+ T cells. We hypothesized that ATF7ip would similarly regulate IL-2 production in CD4+ and CD8+ T cells in other species. In order to test this hypothesis, we utilized the clustered regularly interspaced short palindromic repeats (CRISPR) technology in human CD4+ T cells using three previously published guide RNA's targeting ATF7ip(16). Human CD4+ T cells were chosen because prior studies have shown them to be amenable to CRISPR editing(31, 54). Using anonymous donor T cells, *ATF7ip* deletion in human CD4+ T cells results in increased *IL2* mRNA and enhanced IL-2 secretion after T cell stimulation with anti-CD3 and anti-CD28 (Fig. 5J–5L). To confirm that ATF7ip was deleted with high efficiency, we utilized Synthego's Inference of CRISPR Edits (ICE) analysis. ICE is a web-based program that calculates the percentage of insertions and deletions (indels) introduced by a guide RNA in a CRISPR experiment. A high ICE KO score indicates increased indel formation and an increased likelihood that gene function will be disrupted. We found a high correlation between *ATF7ip* guide RNA ICE KO score and IL-2 production, indicating that if ATF7ip is deleted with high efficiency human CD4+ T cells will produce increased IL-2 with TCR stimulation (Fig. 5L). Thus, ATF7ip appears to have a conserved function across species with ATF7ip deletion in either mouse or human T cells resulting in increased IL-2 production.

Discussion:

In summary, this work establishes a new function for ATF7ip in CD8+ T cell effector function. *CD4*-Cre/*Atf7ip*^fl/fl^ mice have an enhanced ability to clear both primary and secondary LM infections. Notably, the enhanced effector response is dependent on IL-2

as blocking IL-2 with the IL-2 blocking antibody S4B6 abolishes the enhanced effector function. Increased IL-2 levels as the mechanism for the enhanced effector function in *CD4*-Cre/*Atf7ip*^{fl/fl} mice is supported by the literature as IL-2 has been shown to be important in clearing LM infections in mice and in the tumor immune response(55–57). Because *CD4*-Cre/*Atf7ip*^{fl/fl} mice have deletion of ATF7ip in both CD4+ and CD8+ T cells the enhanced effector function may be due to increased IL-2 from CD4+ T cells. Our previous studies have shown that *CD4*-Cre/*Atf7ip*^{fl/fl} T cells produce increased IL-2 with TCR stimulation(30). Furthermore, CD4+ T cells have been shown to be the primary source of IL-2 during an infection and produce significantly more IL-2 than CD8+ T cells. Thus, augmented IL-2 from CD4+ T cells may then act on CD8+ T cells and NK cells to enhance effector function(55). Our data clearly shows that infection of *CD4*-Cre/*Atf7ip*^{fl/fl} mice induces significant transcriptomic changes in CD8+ T cells. Specifically, CD8+ T cells produce increased granzymes and appear to be more metabolically active. Many of these changes may be due to the trans effect of IL-2 from CD4+ T cells acting on CD8+ T cells with multiple studies reporting that CD8+ T cells (unlike CD4+ T cells) are exquisitely sensitive to mitogenic IL-2 signaling with IL-2 promoting CD8+ T cell activation/proliferation and enhancing granzyme production(40–43).

While increased IL-2 appears to be an important driver of the augmented effector response in *CD4*-Cre/*Atf7ip*^{fl/fl} mice, we also found CD8+ T cell intrinsic changes in gene expression with deletion of *Atf7ip*. RNA-seq showed increased expression of genes associated with CD8+ T cell memory such as *Il7r, Eomes*, and *Sell*. Furthermore, utilizing the P14 T cell transfer system we showed that deletion of *Atf7ip* results in increases in both the percentage and absolute number of Il7r+ memory cells. Increased absolute numbers of memory cells may explain the CD8+ T cell intrinsic augmentation of the memory response seen with *Atf7ip* deletion. In addition to increased Il7r expression, *Atf7ip*-deletion in CD8+ T cells also induces increased autocrine IL-2 production. The function of autocrine IL-2 in CD8+ T cells is debated. During a primary response the majority of IL-2 is produced from CD4+ T cells and autocrine IL-2 from CD8+ T cells is dispensable for the initial response to an infection. While not required for primary CD8+ T cell activation, autocrine IL-2 from CD8+ T cells is required for clonal expansion during the memory response suggesting that autocrine IL-2 is important for licensing CD8+ T cell memory(46, 47). Thus, increased autocrine IL-2 with *Atf7ip*-deletion in CD8+ T cells may promote T cell memory along with enhancing clonal expansion of memory cells and potentially increasing the production of effector molecules such as granzymes(43, 44, 53).

ChIP-seq experiments revealed the mechanism of increased *Il7r* expression and *Il2* expression by demonstrating reduced H3K9me3 at the *Il7r* and *Il2-Il21* intergenic region in CD8+ T cells as well as multiple other areas of the genome. Recent studies have shown that ATF7ip's primary function is to modulate the function of the H3K9me3 histone methyltransferase SETDB1(15, 16). In HeLa cells, deletion of ATF7ip or SETDB1 resulted in similar changes in gene expression with multiple ZFPs overexpressed with deletion of either of these proteins(16). Similarly, we found that deletion of ATF7ip in murine CD4+ or CD8+ T cells resulted in increased *ZFP* expression with reduced H3K9me3 at many *ZFP* loci. While there appears to be similar regulation of ZFP in diverse cell types with deletion of ATF7ip or SETDB1, there are also cell type differences. Deletion of *Setdb1* in CD4+

T cells causes a block in thymic T cell development(58) and augmented Th1 priming(59), while deletion of *Atf7ip* in CD4+ T cells causes a defect in Th17 differentiation(30). There have not been any studies of SETDB1 function in CD8+ T cells and future studies will determine if deletion of either *Setdb1* or *Atf7ip* in CD8+ T cells results in similar phenotypes. Why deletion of either *Setdb1* or *Atf7ip* in CD4+ T cells do not result in overlapping phenotypes is unclear as both proteins have a similar function, with *Atf7ip* deletion in CD4+ T cells or CD8+ T cells and *Setdb1* deletion in CD4+ T cells (59) resulting in reduced H3K9me3 deposition at TE. One possible explanation for the divergent phenotypes could be that ATF7ip fine-tunes SETDB1 function and does not completely abolish its enzymatic activity. Another possibility is that either ATF7ip or SETDB1 have other functions in T cells potentially binding to and modulating other proteins. Future studies of ATF7ip and SETDB1 function in T cells will address these possibilities.

Our ChIP-seq data indicates that deletion of *Atf7ip* in either CD4+ T cells or CD8+ T cells results in decreased H3K9me3 deposition at TE. TE comprise approximately 55% of the genome and growing evidence indicates that they are important regulators of gene expression during embryogenesis and in somatic cells(26, 28). In particular, ERVs which comprise 8% of the human genome have been shown to have a number of gene regulatory roles(60). ERVs are the remnants of endogenous retroviruses that have seeded the genome over millions of years. Most ERVs now exist as solitary LTRs that are replication incompetent, however, they still contain binding sites for RNA polymerse II and can induce aberrant transcription of host genes if not silenced through H3K9me3 deposition or CpG methylation. There are a number of examples of ERVs being co-opted for gene regulation in embryonic development. During mouse embryogenesis, zygotic activation genes have been shown to be driven from the LTR of murine endogenous retrovirus L (MERVL) and in humans binding sites for pluripotency factors reside in TE (61–63). Furthermore, in somatic tissues it has been shown that ERVs have been co-opted for the regulation of the placenta and in the immune system for the interferon response, Foxp3 expression, and Th1 responses (59, 64–66). Thus, ERVs are now known to be important regulators of the immune response. Our data shows that deletion of *Atf7ip* results in failure to silence TE and in augmented *Il7r* and *Il2* expression in T cells likely secondary to failed repression of adjacent TE. The increased expression may be due to failure to silence adjacent cis regulatory regions as seen with *Setdb1*-deletion in CD4+ T cells (59), or secondary to increased RNA-polymerase II binding to LTR sequences that were previously silenced. Secondary to the repetitive nature of TE we have been unable to delete TE at specific regions of the genome, however, these studies may begin to be possible with CRISPR. Future studies will determine the exact mechanisms that *Atf7ip*-deletion and failure to silence TE results in aberrant gene expression in T cells.

The finding that there is considerable overlap of sites of H3K9me3 deposition in CD4+ and CD8+ T cells suggests that a portion of TEs may have seeded a murine T cell precursor early in evolution. Moreover, the finding that *IL2* is similarly regulated by ATF7ip in human CD4+ T cells suggests a similar function for this protein between species. Future ChIP-seq experiments after *ATF7ip* deletion in human T cells will address if ATF7ip silences TE at the *IL2* locus in humans. If ATF7ip silences TE at the *IL2* locus in humans, this may suggest a TE that seeded the *IL2* locus early in eukaryotic evolution and was exapted to fine tune

IL-2 expression in eukaryotes. Alternatively, TE may have been selected to target immune response genes in CD8+ T cells to prevent robust immune responses (through increased IL-2) and memory (through increased Il7r) against viral proteins. Future studies studying TE in T cells will interrogate these possibilities.

Our data clearly show that ATF7ip regulates IL-2 in multiple cell types (CD4+ and CD8+ T cells) and multiple species (mouse and human). Future studies will determine if ATF7ip is important for IL-2 production in other cell types such as NK cells(67) and dendritic cells(68) and if Il7r is regulated by ATF7ip in human T cells. Our data shows that enhanced IL-2 production in T cells leads to an increased effector response to infections. Multiple studies have shown the benefits of IL-2 in boosting immune responses to viruses and cancer and high-dose IL-2 has been used in the treatment of cancers such as renal carcinoma and melanoma(56, 57, 69). With the advent of CAR T cell-therapy one could envision future therapeutics deleting ATF7ip in CAR T cells to enhance the effector response to viruses and tumors.

Supplementary Material

Refer to Web version on PubMed Central for supplementary material.

Acknowledgments:

Data Availability -

RNA-seq and ChIP-seq data that support the findings of this study were deposited in GEO with accession numbers: GSE190624 (ChIP-seq) and GSE190417 (RNA-seq) and URLs https://www.ncbi.nlm.nih.gov/geo/query/acc.cgi?acc=GSE190624; https://www.ncbi.nlm.nih.gov/geo/query/acc.cgi?acc=GSE190417.

Non-Standard Abbreviations:

TE	Transposable Elements
Th17	T helper 17
ATF7ip	activating transcription factor 7 interacting protein
MBD1	methyl-CpG binding protein 1

HUSH	human silencing hub
MCAF	MBD1-Containing Chromatin-Associated Factor 1
AM	ATFa-Associated Modulator
EZH2	Enhancer Of Zeste 2 Polycomb Repressive Complex 2 Subunit
SETDB1	SET Domain Bifurcated Histone Lysine Methyltransferase 1
IGV	Integrated Genome Viewer
ZFP	Zinc Finger Protein
ERV	Endogenous Retrovirus
LTR	Long Terminal Repeat

References

1. Kaech SM, Wherry EJ, and Ahmed R. 2002. Effector and memory T-cell differentiation: implications for vaccine development. Nat Rev Immunol 2: 251–262. [PubMed: 12001996]

2. Chang JT, Wherry EJ, and Goldrath AW. 2014. Molecular regulation of effector and memory T cell differentiation. Nat Immunol 15: 1104–1115. [PubMed: 25396352]

3. Williams MA, and Bevan MJ. 2007. Effector and memory CTL differentiation. Annu Rev Immunol 25: 171–192. [PubMed: 17129182]

4. Barata JT, Durum SK, and Seddon B. 2019. Flip the coin: IL-7 and IL-7R in health and disease. Nat Immunol 20: 1584–1593. [PubMed: 31745336]

5. Kaech SM, Tan JT, Wherry EJ, Konieczny BT, Surh CD, and Ahmed R. 2003. Selective expression of the interleukin 7 receptor identifies effector CD8 T cells that give rise to long-lived memory cells. Nat Immunol 4: 1191–1198. [PubMed: 14625547]

6. Joshi NS, Cui W, Chandele A, Lee HK, Urso DR, Hagman J, Gapin L, and Kaech SM. 2007. Inflammation directs memory precursor and short-lived effector CD8(+) T cell fates via the graded expression of T-bet transcription factor. Immunity 27: 281–295. [PubMed: 17723218]

7. Banerjee A, Gordon SM, Intlekofer AM, Paley MA, Mooney EC, Lindsten T, Wherry EJ, and Reiner SL. 2010. Cutting edge: The transcription factor eomesodermin enables CD8+ T cells to compete for the memory cell niche. J Immunol 185: 4988–4992. [PubMed: 20935204]

8. Zhou X, Yu S, Zhao DM, Harty JT, Badovinac VP, and Xue HH. 2010. Differentiation and persistence of memory CD8(+) T cells depend on T cell factor 1. Immunity 33: 229–240. [PubMed: 20727791]

9. Wang Z, Yin H, Lau CS, and Lu Q. 2016. Histone Posttranslational Modifications of CD4(+) T Cell in Autoimmune Diseases. Int J Mol Sci 17.

10. Bulut-Karslioglu A, De La Rosa-Velazquez IA, Ramirez F, Barenboim M, Onishi-Seebacher M, Arand J, Galan C, Winter GE, Engist B, Gerle B, O'Sullivan RJ, Martens JH, Walter J, Manke T, Lachner M, and Jenuwein T. 2014. Suv39h-dependent H3K9me3 marks intact retrotransposons and silences LINE elements in mouse embryonic stem cells. Mol Cell 55: 277–290. [PubMed: 24981170]

11. Kimura H 2013. Histone modifications for human epigenome analysis. J Hum Genet 58: 439–445. [PubMed: 23739122]

12. Schultz DC, Ayyanathan K, Negorev D, Maul GG, and Rauscher FJ 3rd. 2002. SETDB1: a novel KAP-1-associated histone H3, lysine 9-specific methyltransferase that contributes to HP1-mediated silencing of euchromatic genes by KRAB zinc-finger proteins. Genes Dev 16: 919–932. [PubMed: 11959841]

13. Gray SM, Amezquita RA, Guan T, Kleinstein SH, and Kaech SM. 2017. Polycomb Repressive Complex 2-Mediated Chromatin Repression Guides Effector CD8(+) T Cell Terminal Differentiation and Loss of Multipotency. Immunity 46: 596–608. [PubMed: 28410989]

14. Pace L, Goudot C, Zueva E, Gueguen P, Burgdorf N, Waterfall JJ, Quivy JP, Almouzni G, and Amigorena S. 2018. The epigenetic control of stemness in CD8(+) T cell fate commitment. Science 359: 177–186. [PubMed: 29326266]

15. Wang H, Cao R, Xia L, Erdjument-Bromage H, Borchers C, Tempst P, and Zhang Y. 2001. Purification and functional characterization of a histone H3-lysine 4-specific methyltransferase. Mol Cell 8: 1207–1217. [PubMed: 11779497]

16. Timms RT, Tchasovnikarova IA, Antrobus R, Dougan G, and Lehner PJ. 2016. ATF7IP-Mediated Stabilization of the Histone Methyltransferase SETDB1 Is Essential for Heterochromatin Formation by the HUSH Complex. Cell Rep 17: 653–659. [PubMed: 27732843]

17. Fujita N, Watanabe S, Ichimura T, Ohkuma Y, Chiba T, Saya H, and Nakao M. 2003. MCAF mediates MBD1-dependent transcriptional repression. Mol Cell Biol 23: 2834–2843. [PubMed: 12665582]

18. Ichimura T, Watanabe S, Sakamoto Y, Aoto T, Fujita N, and Nakao M. 2005. Transcriptional repression and heterochromatin formation by MBD1 and MCAF/AM family proteins. J Biol Chem 280: 13928–13935. [PubMed: 15691849]

19. Minkovsky A, Sahakyan A, Rankin-Gee E, Bonora G, Patel S, and Plath K. 2014. The Mbd1-Atf7ip-Setdb1 pathway contributes to the maintenance of X chromosome inactivation. Epigenetics Chromatin 7: 12. [PubMed: 25028596]

20. Tchasovnikarova IA, Timms RT, Matheson NJ, Wals K, Antrobus R, Gottgens B, Dougan G, Dawson MA, and Lehner PJ. 2015. GENE SILENCING. Epigenetic silencing by the HUSH complex mediates position-effect variegation in human cells. Science 348: 1481–1485. [PubMed: 26022416]

21. Sasai N, Saitoh N, Saitoh H, and Nakao M. 2013. The transcriptional cofactor MCAF1/ATF7IP is involved in histone gene expression and cellular senescence. PLoS One 8: e68478. [PubMed: 23935871]

22. Turnbull C, Rapley EA, Seal S, Pernet D, Renwick A, Hughes D, Ricketts M, Linger R, Nsengimana J, Deloukas P, Huddart RA, Bishop DT, Easton DF, Stratton MR, Rahman N, and U. K. T. C. Collaboration. 2010. Variants near DMRT1, TERT and ATF7IP are associated with testicular germ cell cancer. Nat Genet 42: 604–607. [PubMed: 20543847]

23. Waterfield M, Khan IS, Cortez JT, Fan U, Metzger T, Greer A, Fasano K, Martinez-Llordella M, Pollack JL, Erle DJ, Su M, and Anderson MS. 2014. The transcriptional regulator Aire coopts the repressive ATF7ip-MBD1 complex for the induction of immunotolerance. Nat Immunol 15: 258–265. [PubMed: 24464130]

24. Fukuda K, Okuda A, Yusa K, and Shinkai Y. 2018. A CRISPR knockout screen identifies SETDB1-target retroelement silencing factors in embryonic stem cells. Genome Res 28: 846–858. [PubMed: 29728365]

25. Matsui T, Leung D, Miyashita H, Maksakova IA, Miyachi H, Kimura H, Tachibana M, Lorincz MC, and Shinkai Y. 2010. Proviral silencing in embryonic stem cells requires the histone methyltransferase ESET. Nature 464: 927–931. [PubMed: 20164836]

26. Bourque G, Burns KH, Gehring M, Gorbunova V, Seluanov A, Hammell M, Imbeault M, Izsvak Z, Levin HL, Macfarlan TS, Mager DL, and Feschotte C. 2018. Ten things you should know about transposable elements. Genome Biol 19: 199. [PubMed: 30454069]

27. Gifford RJ, Blomberg J, Coffin JM, Fan H, Heidmann T, Mayer J, Stoye J, Tristem M, and Johnson WE. 2018. Nomenclature for endogenous retrovirus (ERV) loci. Retrovirology 15: 59. [PubMed: 30153831]

28. Chuong EB, Elde NC, and Feschotte C. 2017. Regulatory activities of transposable elements: from conflicts to benefits. Nat Rev Genet 18: 71–86. [PubMed: 27867194]

29. Imbeault M, Helleboid PY, and Trono D. 2017. KRAB zinc-finger proteins contribute to the evolution of gene regulatory networks. Nature 543: 550–554. [PubMed: 28273063]

30. Sin JH, Zuckerman C, Cortez JT, Eckalbar WL, Erle DJ, Anderson MS, and Waterfield MR. 2019. The epigenetic regulator ATF7ip inhibits Il2 expression, regulating Th17 responses. J Exp Med 216: 2024–2037. [PubMed: 31217192]

31. Cortez JT, Montauti E, Shifrut E, Gatchalian J, Zhang Y, Shaked O, Xu Y, Roth TL, Simeonov DR, Zhang Y, Chen S, Li Z, Woo JM, Ho J, Vogel IA, Prator GY, Zhang B, Lee Y, Sun Z, Ifergan I, Van Gool F, Hargreaves DC, Bluestone JA, Marson A, and Fang D. 2020. CRISPR screen in regulatory T cells reveals modulators of Foxp3. Nature 582: 416–420. [PubMed: 32499641]

32. McCausland MM, and Crotty S. 2008. Quantitative PCR technique for detecting lymphocytic choriomeningitis virus in vivo. J Virol Methods 147: 167–176. [PubMed: 17920702]

33. Cruz-Tapias P, Robin P, Pontis J, Maestro LD, and Ait-Si-Ali S. 2019. The H3K9 Methylation Writer SETDB1 and its Reader MPP8 Cooperate to Silence Satellite DNA Repeats in Mouse Embryonic Stem Cells. Genes (Basel) 10.

34. Dobin A, Davis CA, Schlesinger F, Drenkow J, Zaleski C, Jha S, Batut P, Chaisson M, and Gingeras TR. 2013. STAR: ultrafast universal RNA-seq aligner. Bioinformatics 29: 15–21. [PubMed: 23104886]

35. Love MI, Huber W, and Anders S. 2014. Moderated estimation of fold change and dispersion for RNA-seq data with DESeq2. Genome Biol 15: 550. [PubMed: 25516281]

36. Jin Y, Tam OH, Paniagua E, and Hammell M. 2015. TEtranscripts: a package for including transposable elements in differential expression analysis of RNA-seq datasets. Bioinformatics 31: 3593–3599. [PubMed: 26206304]

37. Li H, and Durbin R. 2009. Fast and accurate short read alignment with Burrows-Wheeler transform. Bioinformatics 25: 1754–1760. [PubMed: 19451168]

38. Zang C, Schones DE, Zeng C, Cui K, Zhao K, and Peng W. 2009. A clustering approach for identification of enriched domains from histone modification ChIP-Seq data. Bioinformatics 25: 1952–1958. [PubMed: 19505939]

39. Zenewicz LA, and Shen H. 2007. Innate and adaptive immune responses to Listeria monocytogenes: a short overview. Microbes Infect 9: 1208–1215. [PubMed: 17719259]

40. Au-Yeung BB, Smith GA, Mueller JL, Heyn CS, Jaszczak RG, Weiss A, and Zikherman J. 2017. IL-2 Modulates the TCR Signaling Threshold for CD8 but Not CD4 T Cell Proliferation on a Single-Cell Level. J Immunol 198: 2445–2456. [PubMed: 28159902]

41. Boyman O, Kovar M, Rubinstein MP, Surh CD, and Sprent J. 2006. Selective stimulation of T cell subsets with antibody-cytokine immune complexes. Science 311: 1924–1927. [PubMed: 16484453]

42. Chinen T, Kannan AK, Levine AG, Fan X, Klein U, Zheng Y, Gasteiger G, Feng Y, Fontenot JD, and Rudensky AY. 2016. An essential role for the IL-2 receptor in Treg cell function. Nat Immunol 17: 1322–1333. [PubMed: 27595233]

43. Pipkin ME, Sacks JA, Cruz-Guilloty F, Lichtenheld MG, Bevan MJ, and Rao A. 2010. Interleukin-2 and inflammation induce distinct transcriptional programs that promote the differentiation of effector cytolytic T cells. Immunity 32: 79–90. [PubMed: 20096607]

44. Kalia V, Sarkar S, Subramaniam S, Haining WN, Smith KA, and Ahmed R. 2010. Prolonged interleukin-2Ralpha expression on virus-specific CD8+ T cells favors terminal-effector differentiation in vivo. Immunity 32: 91–103. [PubMed: 20096608]

45. Redeker A, Welten SP, Baert MR, Vloemans SA, Tiemessen MM, Staal FJ, and Arens R. 2015. The Quantity of Autocrine IL-2 Governs the Expansion Potential of CD8+ T Cells. J Immunol 195: 4792–4801. [PubMed: 26453748]

46. Williams MA, Tyznik AJ, and Bevan MJ. 2006. Interleukin-2 signals during priming are required for secondary expansion of CD8+ memory T cells. Nature 441: 890–893. [PubMed: 16778891]

47. Feau S, Arens R, Togher S, and Schoenberger SP. 2011. Autocrine IL-2 is required for secondary population expansion of CD8(+) memory T cells. Nat Immunol 12: 908–913. [PubMed: 21804558]

48. Cruz-Guilloty F, Pipkin ME, Djuretic IM, Levanon D, Lotem J, Lichtenheld MG, Groner Y, and Rao A. 2009. Runx3 and T-box proteins cooperate to establish the transcriptional program of effector CTLs. J Exp Med 206: 51–59. [PubMed: 19139168]

49. Milner JJ, Toma C, Yu B, Zhang K, Omilusik K, Phan AT, Wang D, Getzler AJ, Nguyen T, Crotty S, Wang W, Pipkin ME, and Goldrath AW. 2017. Runx3 programs CD8(+) T cell residency in non-lymphoid tissues and tumours. Nature 552: 253–257. [PubMed: 29211713]

50. Shan Q, Zeng Z, Xing S, Li F, Hartwig SM, Gullicksrud JA, Kurup SP, Van Braeckel-Budimir N, Su Y, Martin MD, Varga SM, Taniuchi I, Harty JT, Peng W, Badovinac VP, and Xue HH. 2017. The transcription factor Runx3 guards cytotoxic CD8(+) effector T cells against deviation towards follicular helper T cell lineage. Nat Immunol 18: 931–939. [PubMed: 28604718]

51. Wang D, Diao H, Getzler AJ, Rogal W, Frederick MA, Milner J, Yu B, Crotty S, Goldrath AW, and Pipkin ME. 2018. The Transcription Factor Runx3 Establishes Chromatin Accessibility of cis-Regulatory Landscapes that Drive Memory Cytotoxic T Lymphocyte Formation. Immunity 48: 659–674 e656. [PubMed: 29669249]

52. Au-Yeung BB, Shah NH, Shen L, and Weiss A. 2018. ZAP-70 in Signaling, Biology, and Disease. Annu Rev Immunol 36: 127–156. [PubMed: 29237129]

53. Kalia V, and Sarkar S. 2018. Regulation of Effector and Memory CD8 T Cell Differentiation by IL-2-A Balancing Act. Front Immunol 9: 2987. [PubMed: 30619342]

54. Roth TL, Puig-Saus C, Yu R, Shifrut E, Carnevale J, Li PJ, Hiatt J, Saco J, Krystofinski P, Li H, Tobin V, Nguyen DN, Lee MR, Putnam AL, Ferris AL, Chen JW, Schickel JN, Pellerin L, Carmody D, Alkorta-Aranburu G, Del Gaudio D, Matsumoto H, Morell M, Mao Y, Cho M, Quadros RM, Gurumurthy CB, Smith B, Haugwitz M, Hughes SH, Weissman JS, Schumann K, Esensten JH, May AP, Ashworth A, Kupfer GM, Greeley SAW, Bacchetta R, Meffre E, Roncarolo MG, Romberg N, Herold KC, Ribas A, Leonetti MD, and Marson A. 2018. Reprogramming human T cell function and specificity with non-viral genome targeting. Nature 559: 405–409. [PubMed: 29995861]

55. Haak-Frendscho M, Young KM, and Czuprynski CJ. 1989. Treatment of mice with human recombinant interleukin-2 augments resistance to the facultative intracellular pathogen Listeria monocytogenes. Infect Immun 57: 3014–3021. [PubMed: 2789191]

56. Rosenberg SA 2014. IL-2: the first effective immunotherapy for human cancer. J Immunol 192: 5451–5458. [PubMed: 24907378]

57. West EE, Jin HT, Rasheed AU, Penaloza-Macmaster P, Ha SJ, Tan WG, Youngblood B, Freeman GJ, Smith KA, and Ahmed R. 2013. PD-L1 blockade synergizes with IL-2 therapy in reinvigorating exhausted T cells. J Clin Invest 123: 2604–2615. [PubMed: 23676462]

58. Takikita S, Muro R, Takai T, Otsubo T, Kawamura YI, Dohi T, Oda H, Kitajima M, Oshima K, Hattori M, Endo TA, Toyoda T, Weis J, Shinkai Y, and Suzuki H. 2016. A Histone Methyltransferase ESET Is Critical for T Cell Development. J Immunol 197: 2269–2279. [PubMed: 27511731]

59. Adoue V, Binet B, Malbec A, Fourquet J, Romagnoli P, van Meerwijk JPM, Amigorena S, and Joffre OP. 2019. The Histone Methyltransferase SETDB1 Controls T Helper Cell Lineage Integrity by Repressing Endogenous Retroviruses. Immunity 50: 629–644 e628. [PubMed: 30737147]

60. Lander ES, Linton LM, Birren B, Nusbaum C, Zody MC, Baldwin J, Devon K, Dewar K, Doyle M, FitzHugh W, Funke R, Gage D, Harris K, Heaford A, Howland J, Kann L, Lehoczky J, LeVine R, McEwan P, McKernan K, Meldrim J, Mesirov JP, Miranda C, Morris W, Naylor J, Raymond C, Rosetti M, Santos R, Sheridan A, Sougnez C, Stange-Thomann Y, Stojanovic N, Subramanian A, Wyman D, Rogers J, Sulston J, Ainscough R, Beck S, Bentley D, Burton J, Clee C, Carter N, Coulson A, Deadman R, Deloukas P, Dunham A, Dunham I, Durbin R, French L, Grafham D, Gregory S, Hubbard T, Humphray S, Hunt A, Jones M, Lloyd C, McMurray A, Matthews L, Mercer S, Milne S, Mullikin JC, Mungall A, Plumb R, Ross M, Shownkeen R, Sims S, Waterston RH, Wilson RK, Hillier LW, McPherson JD, Marra MA, Mardis ER, Fulton LA, Chinwalla AT, Pepin KH, Gish WR, Chissoe SL, Wendl MC, Delehaunty KD, Miner TL, Delehaunty A, Kramer JB, Cook LL, Fulton RS, Johnson DL, Minx PJ, Clifton SW, Hawkins T, Branscomb E, Predki P, Richardson P, Wenning S, Slezak T, Doggett N, Cheng JF, Olsen A, Lucas S, Elkin C, Uberbacher E, Frazier M, Gibbs RA, Muzny DM, Scherer SE, Bouck JB, Sodergren EJ, Worley KC, Rives CM, Gorrell JH, Metzker ML, Naylor SL, Kucherlapati RS, Nelson DL, Weinstock GM, Sakaki Y, Fujiyama A, Hattori M, Yada T, Toyoda A, Itoh T, Kawagoe C, Watanabe H, Totoki Y, Taylor T, Weissenbach J, Heilig R, Saurin W, Artiguenave F, Brottier P, Bruls T, Pelletier E, Robert C, Wincker P, Smith DR, Doucette-Stamm L, Rubenfield M, Weinstock K, Lee HM, Dubois J,

Rosenthal A, Platzer M, Nyakatura G, Taudien S, Rump A, Yang H, Yu J, Wang J, Huang G, Gu J, Hood L, Rowen L, Madan A, Qin S, Davis RW, Federspiel NA, Abola AP, Proctor MJ, Myers RM, Schmutz J, Dickson M, Grimwood J, Cox DR, Olson MV, Kaul R, Raymond C, Shimizu N, Kawasaki K, Minoshima S, Evans GA, Athanasiou M, Schultz R, Roe BA, Chen F, Pan H, Ramser J, Lehrach H, Reinhardt R, McCombie WR, de la Bastide M, Dedhia N, Blocker H, Hornischer K, Nordsiek G, Agarwala R, Aravind L, Bailey JA, Bateman A, Batzoglou S, Birney E, Bork P, Brown DG, Burge CB, Cerutti L, Chen HC, Church D, Clamp M, Copley RR, Doerks T, Eddy SR, Eichler EE, Furey TS, Galagan J, Gilbert JG, Harmon C, Hayashizaki Y, Haussler D, Hermjakob H, Hokamp K, Jang W, Johnson LS, Jones TA, Kasif S, Kaspryzk A, Kennedy S, Kent WJ, Kitts P, Koonin EV, Korf I, Kulp D, Lancet D, Lowe TM, McLysaght A, Mikkelsen T, Moran JV, Mulder N, Pollara VJ, Ponting CP, Schuler G, Schultz J, Slater G, Smit AF, Stupka E, Szustakowki J, Thierry-Mieg D, Thierry-Mieg J, Wagner L, Wallis J, Wheeler R, Williams A, Wolf YI, Wolfe KH, Yang SP, Yeh RF, Collins F, Guyer MS, Peterson J, Felsenfeld A, Wetterstrand KA, Patrinos A, Morgan MJ, de Jong P, Catanese JJ, Osoegawa K, Shizuya H, Choi S, Chen YJ, Szustakowki J, and C. International Human Genome Sequencing. 2001. Initial sequencing and analysis of the human genome. Nature 409: 860–921. [PubMed: 11237011]

61. Bourque G, Leong B, Vega VB, Chen X, Lee YL, Srinivasan KG, Chew JL, Ruan Y, Wei CL, Ng HH, and Liu ET. 2008. Evolution of the mammalian transcription factor binding repertoire via transposable elements. Genome Res 18: 1752–1762. [PubMed: 18682548]

62. Dupressoir A, Lavialle C, and Heidmann T. 2012. From ancestral infectious retroviruses to bona fide cellular genes: role of the captured syncytins in placentation. Placenta 33: 663–671. [PubMed: 22695103]

63. Fort A, Hashimoto K, Yamada D, Salimullah M, Keya CA, Saxena A, Bonetti A, Voineagu I, Bertin N, Kratz A, Noro Y, Wong CH, de Hoon M, Andersson R, Sandelin A, Suzuki H, Wei CL, Koseki H, F. Consortium, Hasegawa Y, Forrest AR, and Carninci P. 2014. Deep transcriptome profiling of mammalian stem cells supports a regulatory role for retrotransposons in pluripotency maintenance. Nat Genet 46: 558–566. [PubMed: 24777452]

64. Chuong EB, Elde NC, and Feschotte C. 2016. Regulatory evolution of innate immunity through co-option of endogenous retroviruses. Science 351: 1083–1087. [PubMed: 26941318]

65. Chuong EB, Rumi MA, Soares MJ, and Baker JC. 2013. Endogenous retroviruses function as species-specific enhancer elements in the placenta. Nat Genet 45: 325–329. [PubMed: 23396136]

66. Samstein RM, Josefowicz SZ, Arvey A, Treuting PM, and Rudensky AY. 2012. Extrathymic generation of regulatory T cells in placental mammals mitigates maternal-fetal conflict. Cell 150: 29–38. [PubMed: 22770213]

67. Malek TR 2008. The biology of interleukin-2. Annu Rev Immunol 26: 453–479. [PubMed: 18062768]

68. Zelante T, Fric J, Wong AY, and Ricciardi-Castagnoli P. 2012. Interleukin-2 production by dendritic cells and its immuno-regulatory functions. Front Immunol 3: 161. [PubMed: 22719740]

69. Blattman JN, Grayson JM, Wherry EJ, Kaech SM, Smith KA, and Ahmed R. 2003. Therapeutic use of IL-2 to enhance antiviral T-cell responses in vivo. Nat Med 9: 540–547. [PubMed: 12692546]

Key Points:

- ATF7ip is a critical regulator of CD8+ T cell effector and memory responses.

- Deletion of ATF7ip in CD8+ T results in enhanced *Il2* and *Il7r* expression.

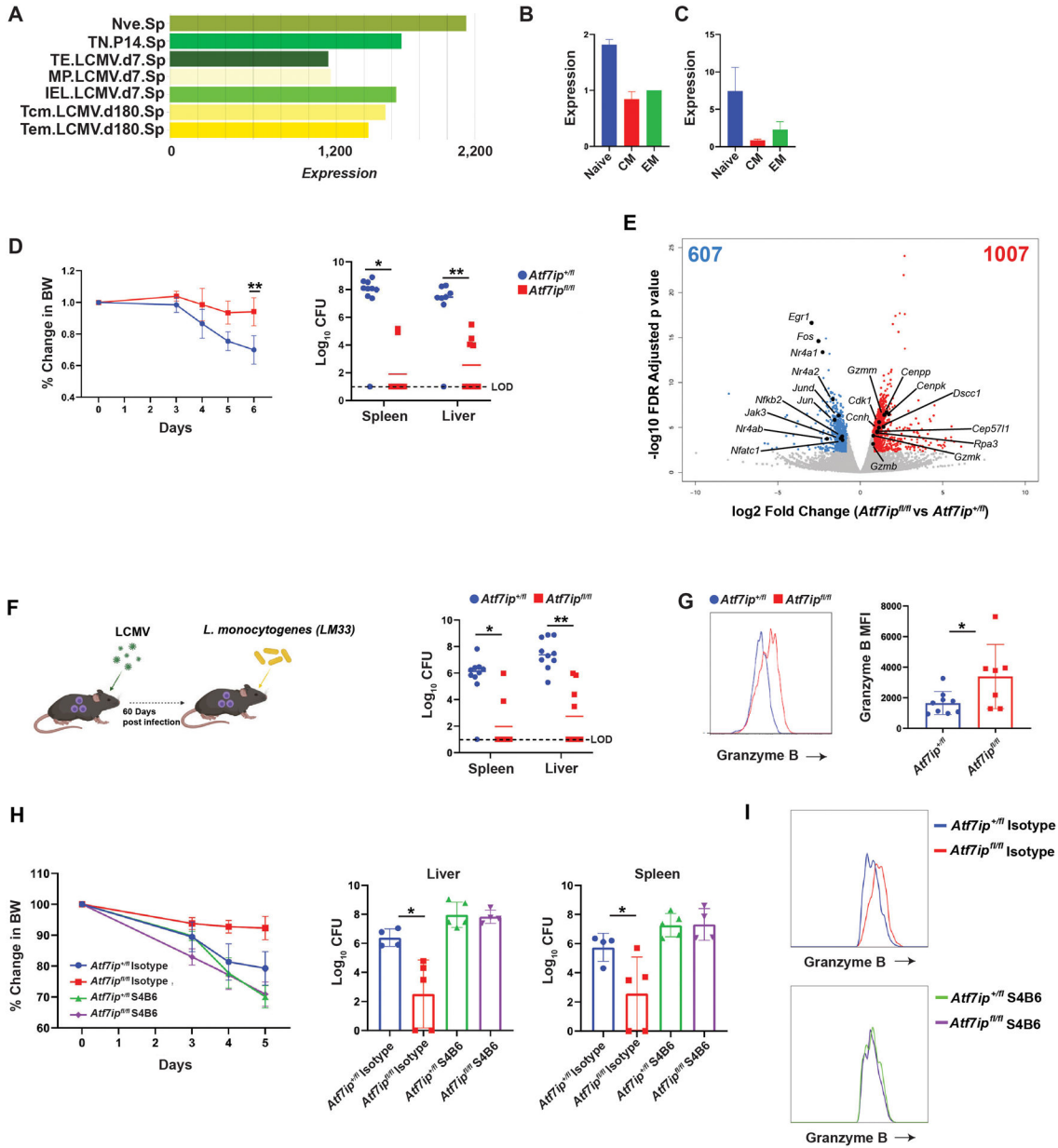- ATF7ip targets transposable elements to modulate *Il7r* and *Il2* expression.

Figure 1 –. IL-2 is required for resistance to infection in *CD4*-Cre/*ATF7ip*^fl/fl mice.
(**A**) Relative expression of *Atf7ip* mRNA in CD8+ T cells from spleens infected with LCMV. Downloaded from the Immgen expression database. (**B-C**) Relative expression of *Atf7ip* mRNA in CD8+ T cell subsets (**B**) or naïve CD8+ T cells (**C**) stimulated with anti-CD3 (2ug) and anti-CD28 (2ug) for the indicated times. (**D**) *CD4*-Cre/*Atf7ip*^+/fl (*Atf7ip*^+/fl) mice and *CD4*-Cre/*Atf7ip*^fl/fl (*Atf7ip*^fl/fl) mice were infected i.v. with a lethal dose (2×10^4 CFU) of Listeria monocytogenes and analyzed for body weight change and spleen/liver bacterial load (colony counts) 6 days post infection. (**E**) Volcano plot of RNA-seq data comparing global gene expression analysis in LCMV specific CD8+ T cells from *CD4*-Cre/*Atf7ip*^+/fl (*Atf7ip*^+/fl) and *CD4*-Cre/*Atf7ip*^fl/fl (*Atf7ip*^fl/fl) mice infected with LCMV Armstrong. CD8+ T cells were isolated by flow cytometry using the LCMV specific

tetramer GP33 (CD8+CD44+GP33+). Red numbers indicate the number of genes that are significantly increased (FDR < 0.01, log2fold > 0.75) in *CD4*-Cre/*Atf7ip*$^{fl/fl}$ CD8+ T cells, and blue numbers indicated the number of genes that are significantly increased in *CD4*-Cre/*Atf7ip*$^{+/fl}$ (*Atf7ip*$^{+/fl}$) CD8+ T cells. RNA-seq analysis was performed in triplicate. **(F)** Experimental setup testing CD8+ T cell memory responses. *CD4*-Cre/*Atf7ip*$^{+/fl}$ (*Atf7ip*$^{+/fl}$) and *CD4*-Cre/*Atf7ip*$^{fl/fl}$ (*Atf7ip*$^{fl/fl}$) mice were aged and sex matched and infected i.p. with LCMV-Armstrong followed by a secondary i.v. infection (Day 60 post LMCV infection) with an LM strain expressing the LCMV H2D^b epitope GP$_{33-41}$ (LM33, 1×10^6 CFU). Spleen/Liver bacterial load (colony counts) 3 days after i.v. LM33 infection. **(G)** Granzyme B expression in CD8+CD44+GP33+ cells three days after reinfection with LM33. **(H-I)** *CD4*-Cre/*Atf7ip*$^{+/fl}$ (*Atf7ip*$^{+/fl}$) and *CD4*-Cre/*Atf7ip*$^{fl/fl}$ (*Atf7ip*$^{fl/fl}$) mice were treated with anti-IL2 antibody (Clone S4B6–1) or with IgG2a isotype control and infected with 2×10^4 CFU LM33. Mice received 150ug of isotype or S4B6 on Day −1, Day 1, and Day 3 with LM33 infections at Day 0. **(H)** Body weights of mice were taken on Day 0 and on Days 3, 4, and 5. Spleen/Liver bacterial load (colony counts) 5 days after LM33 infection. **(I)** Granzyme B expression in CD8+CD44+GP33+ cells at day 5. Each data point in (D, F, G, and H) represents an individual mouse. Data in (D, F, and G) are the combination of two experiments with 7–10 mice per genotype in each group. Data in H is one representative experiment of two experiments with 4–5 mice per group. Error bars (B, C, D, G, and H) show mean with SD. * P < 0.05, ** P < 0.01 by Student's *t* test. LOD = limit of detection.
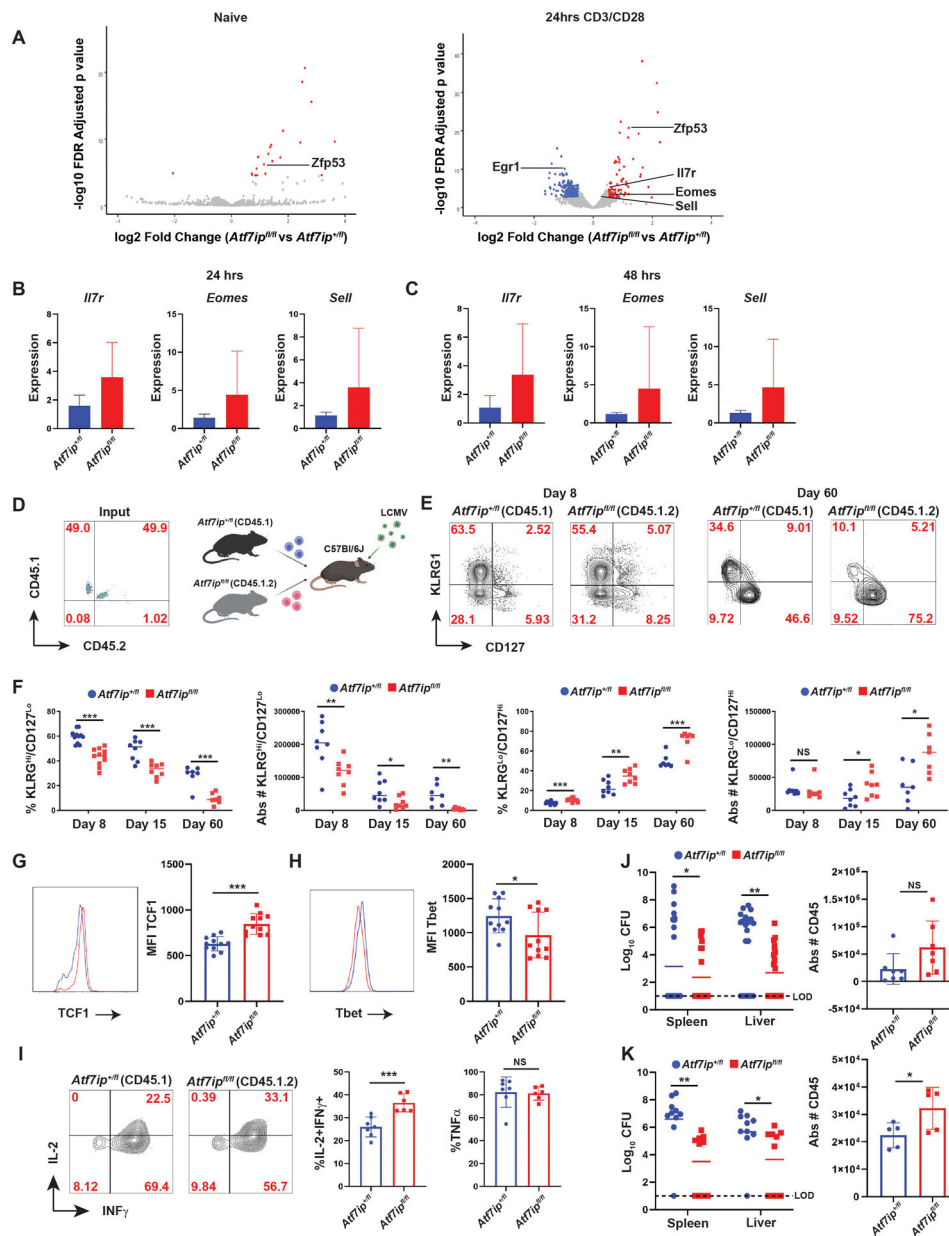
Figure 2 –. Deletion of *Atf7ip* results in a CD8+ T cell intrinsic increase in *Il7r* expression
(A) Volcano plots from RNA-seq data comparing global gene expression analysis in CD8+ T cells from *CD4*-Cre/*Atf7ip+/fl* and *CD4*-Cre/*Atf7ipfl/fl* mice. Left plot represents naïve CD8+ T cells and right plot represents naïve CD8+ T cells *in vitro* stimulated for 24 hours with anti-CD3 (2ug) and anti-CD28 (2ug). RNA-seq was performed in triplicate. **(B-C)** Relative gene expression of *Il7r, Eomes*, and *Sell* from CD8+ T cells stimulated with anti-CD3 (2ug) and anti-CD28 (2ug) for 24hrs **(B)** or 48hrs **(C)**. **(D-F)** 2×10^4 P14+/CD45.1.2/ *Atf7ipfl/fl* CD8+ T cells and P14+/CD45.1/*Atf7ip+/fl* CD8+ T cells were co-transferred into CD45.2 C57Bl/6 hosts 1 day prior to LCMV infection. **(D)** Representative flow cytometry of input P14+ T cells prior to transfer into CD45.2 C57Bl/6 hosts. **(E)** Flow cytometry analysis of splenic CD8+ T cells stained for CD8+/CD44+/CD45.1+/CD45.2+/ KLRG1+/

CD127+ at 8 and 60 days after transfer. Red numbers indicate the percentage of cells in each gate. **(F)** Percentage and absolute # of P14+ positive KLRG1^Hi/CD127^Lo terminal effectors and KLRG1^Lo/CD127^Hi memory cells in the spleen 8, 15 and 60 days after infection. **(G-H)** TCF1 **(G)** and Tbet **(H)** expression at day 60 post transfer. **(I)** Intracellular cytokine staining of P14+ cells day 60 post infection. Cells were stimulated with GP33 peptide for 5hrs prior to FACS analysis. **(J)** Experimental setup outlined in Supplemental Fig. 2E. 2 × 10^4 P14+/CD45.1.2/*Atf7ip^fl/fl* CD8+ T cells or P14+/CD45.1/*Atf7ip^+/fl* CD8+ T cells were individually transferred into CD45.2 C57Bl/6 hosts 1 day prior to LCMV infection. 60 days after LCMV infection mice were infected with 1×10^6 LM33 i.v. and spleen/liver CFU were measured three days post LM33 infection. Bar graph depicts absolute number of CD8+CD44+CD45.1+ or CD8+CD44+CD45.1.2+ T cells in the spleen after LM33 infection. **(K)** Experimental setup outlined in Supplemental Fig. 2F. 2 × 10^4 P14+/CD451.2/ *Atf7ip^fl/fl* CD8+ T cells and P14+/CD45.1/*Atf7ip^+/fl* CD8+ T cells were co-transferred into CD45.2 C57Bl/6 hosts 1 day prior to LCMV infection. After 60 days, CD45.1 and CD45.1.2 CD8+ memory cells were flow sorted and 3×10^4 cells of each genotype were transferred IV into naïve B6 mice one day prior to infection with 8 × 10^4 CFU LM33. Spleen/liver CFU were measured five days post LM33 infection. Bar graph depicts absolute number of CD8+CD44+CD45.1+ or CD8+CD44+CD451.2+ T cells in the spleen after LM33 infection. Data in (F-K) are the combination of two experiments with 5–20 mice per genotype in each group with each data point representing an individual mouse. Error bars (B,C) show mean with SEM. Error bars (F-K) show mean with SD. * P < 0.05, ** P < 0.01, *** P< 0.001 by Student's *t* test. NS = non-significant. LOD = limit of detection.

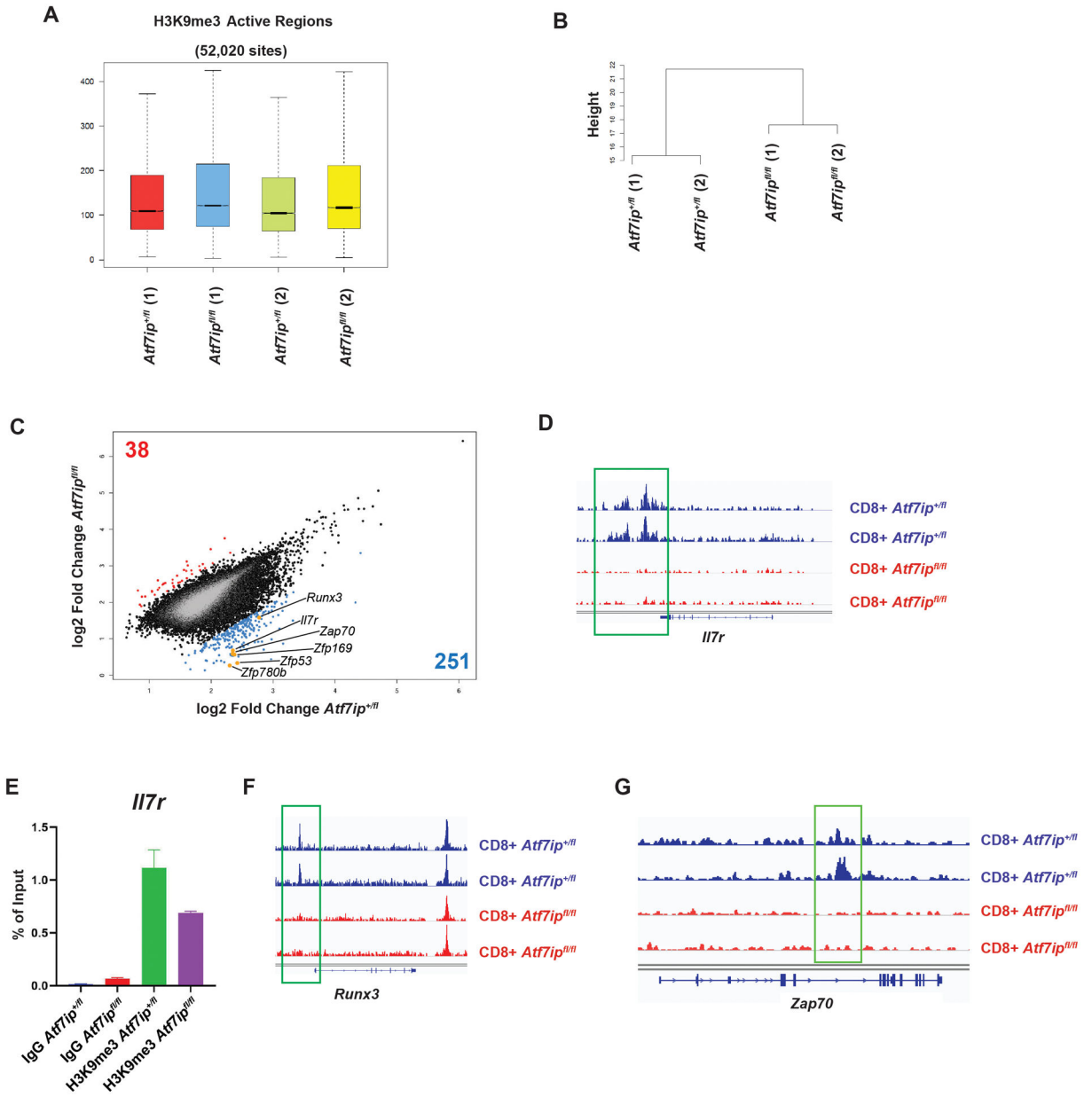**Figure 3 –. ATF7ip is required for H3K9me3 deposition at the *Il7r*.**
(A to G) H3K9me3 ChIP-seq was performed in duplicate in *CD4*-Cre/*Atf7ip^+/fl* (*Atf7ip^+/fl*) and *CD4*-Cre/*Atf7ip^fl/fl* (*Atf7ip^fl/fl*) naïve CD8+ T cells. Numbers in parenthesis indicate sample number for a specific genotype. **(A)** Peak tag number boxplots for individual ChIP-seq samples **(B)** Sample clustering of individual H3K9me3 ChIP-seq samples. **(C)** Scatterplot comparing log2 fold change of H3K9me3 in *CD4*-Cre/*Atf7ip^+/fl* (*Atf7ip^+/fl*) and *CD4*-Cre/*Atf7ip^fl/fl* (*Atf7ip^fl/fl*) naïve CD8+ T cells. Blue numbers represent the number of loci with two-fold increased H3K9me3 in *CD4*-Cre/*Atf7ip^+/fl* naïve CD8+ T cells compared to *CD4*-Cre/*Atf7ip^fl/fl* naïve CD8+ T cells. Red numbers indicate the number of loci with two-fold increased H3K9me3 in *CD4*-Cre/*Atf7ip^fl/fl* naïve CD8+ T cells. **(D)** Integrated genome viewer (IGV) H3K9me3 ChIP-seq tracings for *Il7r*. **(E)** H3K9me3 ChIP qPCR

targeting the site of H3K9me3 deposition within the *Il7r* gene. (**F**) IGV H3K9me3 ChIP-seq tracings for *Runx3*. (**G**) IGV H3K9me3 ChIP-seq tracings for *Zap70*.
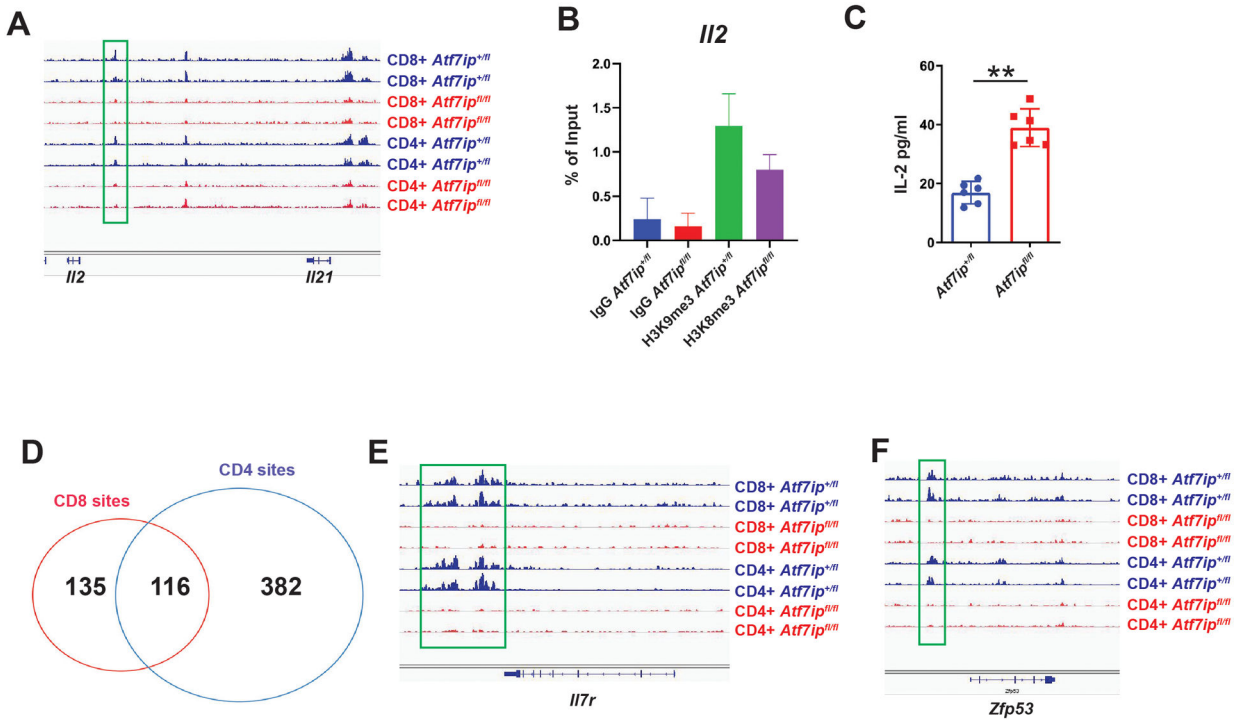
Figure 4 –. ATF7ip targets similar loci for H3K9me3 deposition in naïve CD4+ and CD8+ T cells.
(A) IGV H3K9me3 ChIP-seq tracings for the *Il2-Il21* intergenic region in naïve CD8+ and naïve CD4+ T cells. **(B)** H3K9me3 ChIP qPCR targeting the site of H3K9me3 deposition within the *Il2* gene of naïve CD8+ T cells. **(C)** Naïve CD8+ T cells were stimulated for 24 hours in the presence of TCR stimulation (2ug anti-CD3) and costimulation (2ug anti-CD28) and an IL-2 ELISA was performed from culture supernatant. **(D)** Venn Diagram showing overlap of ChIP-seq sites of ATF7ip-dependent H3K9me3 deposition in naïve CD4+ T cells and naïve CD8+ T cells. **(E)** IGV H3K9me3 ChIP-seq tracings for the *Il7r* gene in naïve CD8+ and naïve CD4+ T cells. **(F)** IGV H3K9me3 ChIP-seq tracings for the *Zfp53* gene in naïve CD8+ and naïve CD4+ T cells. Green boxes show sites of two-fold decreased H3K9me3 deposition. Each data point represents an individual mouse. Data in (C) is representative of two experiments with 3 mice per genotype. Error bars mean with SD. ** $p<0.01$ by Studen s T test.
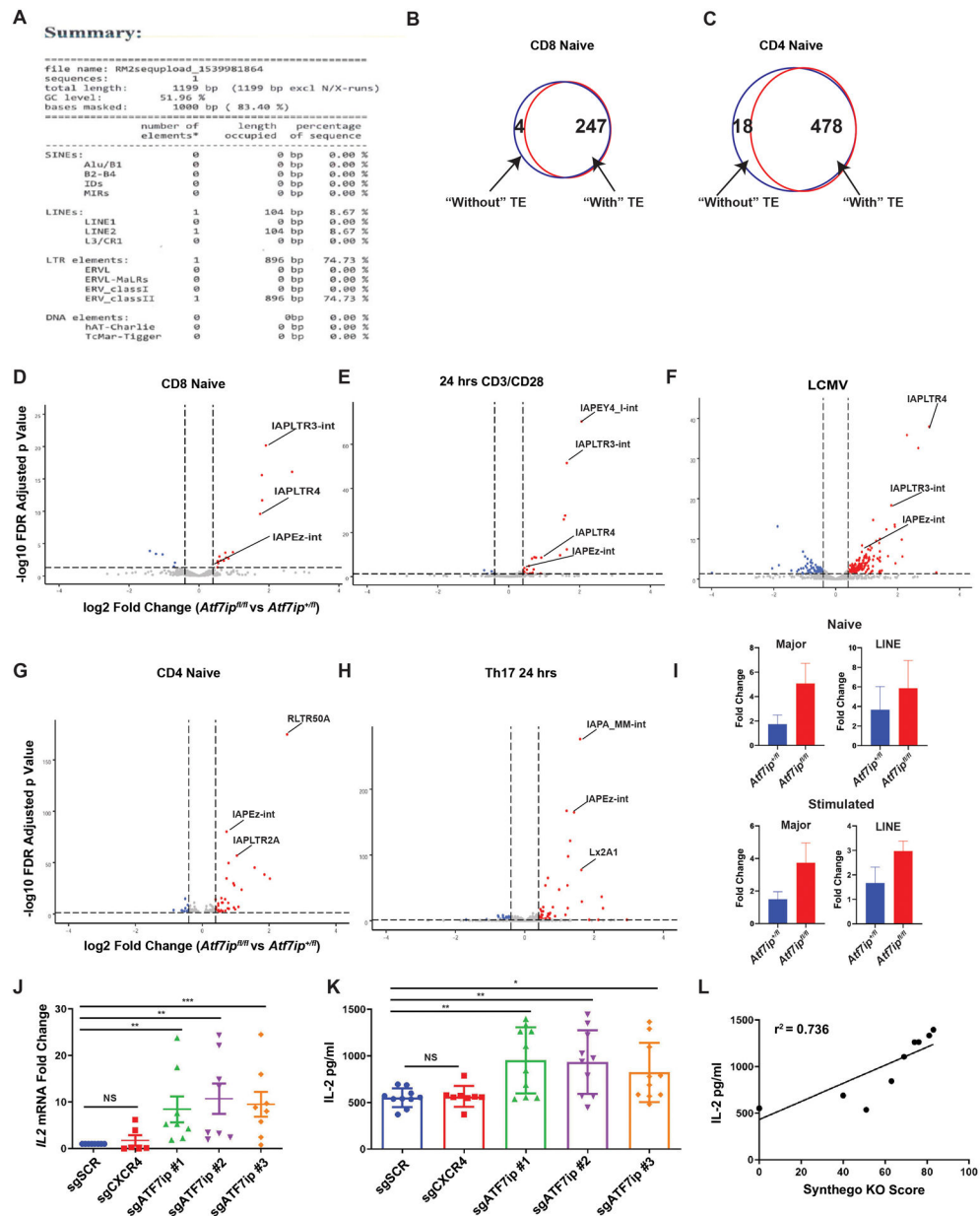
Figure 5 –. ATF7ip targets transposable elements (TE) for H3K9me3 deposition.
(**A**) Repeatmasker output of TE located at the 1199 bp site of ATF7ip-dependent H3K9me3 deposition in the *Il2-Il21* intergenic region. (**B-C**) Overlap of TE and sites of ATF7ip-dependent H3K9me3 deposition in (**B**) naïve CD8+ and (**C**) naïve CD4+ T cells. Red circles depict ChIP-seq sites with TE and blue circles depict total ChIP-seq sites. (**D-H**) Analysis of RNA-seq data using TE transcripts. Red circles indicate TE that are significantly increased (FDR < 0.05, log2fold > 0.4) in *CD4*-Cre/*Atf7ip^{fl/fl}* T cells, and blue circles indicate TE that are significantly increased in *CD4*-Cre/*Atf7ip^{+/fl}* (*Atf7ip^{+/fl}*) T cells (FDR < 0.05, log2fold > 0.4). RNA-seq analysis was performed in triplicate. (**D**) Naïve CD8+ T cells, (**E**) Naïve CD8+ T cells stimulated with anti-CD3 (2ug) and anti-CD28 (2ug), (**F**) Analysis of data from Fig. 1E on CD8+CD44+GP33+ T cells from LCMV infected *CD4*-Cre/*Atf7ip^{+/fl}*

($Atf7ip^{+/fl}$) and $CD4$-Cre/$Atf7ip^{fl/fl}$ ($Atf7ip^{fl/fl}$) mice, **(G)** Naïve CD4+ T cells, and **(H)** Naïve CD4+ T cells in vitro stimulated under Th17 inducing conditions with for 24hrs. **(I)** qPCR for TE expression in naïve CD8+ T cells and CD8+ T cells stimulated for 24hrs with anti-CD3 and anti-CD28. Primers used annealed to conserved sequences in the major satellite DNA repeats of ERVs (Major) and LINE elements (LINE). **(J-L)** CRISPR in human CD4+ T cells with a scrambled guide RNA (*sg SCR*), a CXCR4 guide RNA (*sgCXCR4*), or three different *ATF7ip* guide RNA (*sgATF7ip*). The *sgCXCR4* was included as a cutting control. **(J)** qPCR for *IL2* mRNA. **(K)** ELISA to quantitate secreted IL-2. **(L)** Correlation of ICE KO score for *sgATF7ip#1* vs IL-2 secretion. Each data point represents an individual donor. *p<0.05, **p<0.01.